

Coherent energy migration in solids. I. Band-trap equilibria at Boltzmann and non-Boltzmann temperatures

M. D. Fayer and C. B. Harris*

Department of Chemistry, University of California, Berkeley, California 94720

Inorganic Materials Research Division, Lawrence Berkeley Laboratory, Berkeley, California 94720

(Received 21 May 1973)

A model is presented which relates the dynamics of energy migration in crystals to the mechanism by which thermal equilibrium between delocalized band states and localized trap states is achieved. Central to this model is the requirement that coherent energy migration must be the dominant mode of migration at low temperatures in order to achieve Boltzmann equilibrium between band and trap states within the lifetime of the excited electronic state. Second, a stochastic model for detrapping is developed which is based on an irreversible radiationless relaxation process of a phonon-trap intermediate into the density of delocalized band states. Explicit account is taken of phonon-trap interactions in the formation of the excited trap intermediate. Further, the relation between detrapping and the ability of a crystal to achieve thermal equilibrium within the excited-state lifetime is developed and applied to one-dimensional crystals. Experimental results on molecular crystals representing examples of one-dimensional exciton bands are also presented. Specifically, the temperature dependence of phosphorescence from excited triplet trap states is interpreted in terms of the above considerations. From these experiments one can obtain both the sign of the intermolecular interaction and the dispersion of the first excited triplet band in addition to an estimate of the coherence length associated with exciton migration in the Frenkel limit. Finally, some new and unique methods for studying energy migration are presented which utilize optically detected magnetic-resonance techniques in zero field. They include experiments based on the measurement of electron-spin coherence in the rotating frame and the relationship of the spin coherence to the various rate processes important in trap-exciton interactions.

I. INTRODUCTION

In this paper, the relation between energy migration in solids and the populations of localized and delocalized states will be discussed in terms of a model which includes explicit features of the exciton band, the sign of the intermolecular interaction in the nearest-neighbor approximation, the number of wave-vector states comprising the band, and a mechanism for Frenkel¹ exciton migration in solids including the effects of coherent and incoherent propagation. Although the theoretical and experimental details which will be presented here pertain to the triplet state of molecular solids, identical considerations are also applicable to singlet states and transport phenomena in nonmolecular solids. The model will be applied specifically to the temperature dependence of the intensity of trap emission in molecular crystals although the approach is applicable to a wide variety of related problems.

The necessity of considering the above features of exciton migration in solids in a model which attempts to explain some straightforward observations on the temperature dependence of the intensity of the trap states can readily be seen by the paradoxes which are created if exciton dynamics are not treated properly. For illustration consider the simplest case, where it is tacitly assumed that the excited states of the host are degenerate and that

the different types of traps which may be due either to impurities or crystal lattice defects may be regarded as independent but describable by Boltzmann statistics. The problems created by this oversimplified treatment can readily be seen. In the absence of intermolecular interactions between an excited host molecule and its unexcited neighbors, an excitation is an isolated molecular state as opposed to a mobile crystal state, and hence it cannot migrate to a trap. The difficulty of this model is not so much in the trivial assumption that the host states are degenerate (i. e., no intermolecular interactions) but *in failing to provide a mechanism whereby thermal equilibrium between the host and trap states can be achieved which permits the use of Boltzmann statistics.*² This latter consideration requires that a distinction be made between coherent and incoherent migration insofar as the dynamics of achieving trap-exciton equilibration determine whether or not Boltzmann statistics are a valid assumption. Intermolecular interactions break the degeneracy of the host excited states and produce a band of mobile exciton states with width 4β , where β is the intermolecular interaction matrix element. These mobile excitons can migrate between traps, in one limit (the low-temperature limit), as a coherent wave packet whose properties are determined by the wave vectors of the crystals or, in another limit (high-temperature limit), as a random-walk diffusional process characterized by

a hopping frequency proportional to the intermolecular interaction.³ If the migration is rapid, equilibration of the excited-state populations can be established among the exciton and trap states within the lifetime of the excited electronic state. The populations of the various energy levels can then be determined using a Boltzmann statistical model. The width of the exciton band and the sign of the intermolecular interaction, the location of the exciton energy levels relative to the trap depth, and the mode of exciton migration all determine whether or not the equilibrium condition can be established within the lifetime of the state, and hence determine the functional form of the temperature dependence of the trap emission. Indeed, we shall demonstrate that the measurement of trap phosphorescence, which reflects the triplet-trap population, provides a tool capable of investigating the mode of migration in triplet Frenkel excitons in addition to the magnitude and sign of the intermolecular interaction β .

Specifically in the following, the temperature dependence of trap phosphorescence will be discussed using a model which primarily treats the exciton band as one-dimensional, although multi-dimensional bands are considered briefly. A method for determining the exciton bandwidth and the sign of β from the trap-emission temperature dependence is presented. Systems composed of both single and multiple traps in equilibrium with an exciton band will be considered where the effect of coherent versus random-walk exciton migration on the temperature dependence of the trap-emission intensity is central to the model. Next we will discuss isotopically mixed crystals where the effects of trapping result in both a Boltzmann equilibration and non-Boltzmann equilibration in different temperature regions. Solutions to the non-Boltzmann steady state between trap and band states also allow a measure of the coherence to be estimated. In addition, a model for the decay of localized states into delocalized band states based on radiationless relaxation is developed. Finally, experimental results on "one-dimensional" molecular crystals will be presented and interpreted in terms of the above considerations. These include optically detected magnetic-resonance experiments on trap states in which the electron-spin coherence in the rotating frame is used to measure absolute detrapping rates.

II. THERMAL EQUILIBRIA BETWEEN EXCITON STATES AND SINGLE TRAPS

The formal features of one-dimensional Frenkel excitons in the absence of phonon-exciton coupling are well understood.⁴ A finite linear array of n independent molecules in which one molecule of the chain is in an excited electronic state will have an

energy E^0 corresponding to the "isolated" molecular excited-state energy. The system, however, is n -fold degenerate, since the excitation may be on any one of the n molecules in the linear array. If the molecules are allowed to interact through a nearest-neighbor interaction β , the degeneracy is destroyed and a band of energies is formed. In the nearest-neighbor approximation the energy dependence of the exciton band on the quantum number k , which labels the levels, is given by

$$E(k) = E_0 + 2\beta \cos ka, \quad (2.1)$$

where a is the distance between translationally equivalent molecules along the axis of delocalization. The quantum number k can take on n values from 0 to $\pm\pi/a$ in the first Brillouin zone, giving a bandwidth of 4β .

The temperature dependence of the intensity of trap emission in the temperature region where Boltzmann statistics is applicable can be understood in terms of the partition function z for the systems consisting of one excitation found either in the trap energy level or in one of the levels of the exciton band. We adopt as a model for "real" one-dimensional crystals a crystal composed of a set of independent exciton chains, each chain being separated by one or more impurities or trap sites. The Gaussian distribution of chain lengths in a crystal is sharply peaked, and therefore the average length is employed. This is a valid assumption for most bands provided the number of molecules in a chain exceeds ~ 100 . Each chain may be labeled by a set of molecular indices which specify its location in the crystal and thus make it distinguishable from the other chains in the crystal. This, in addition to the fact that there are many energy levels available to each excitation in the crystal, allows Boltzmann statistics to be employed in writing the partition function *provided the trap and band states are in thermal equilibrium*. Such a partition function has the form

$$z = 1 + e^{-\Delta/kT} + \sum_{k=\pi/na}^{(n-1)(\pi/na)} 2e^{-[\Delta - 2\beta(1 - \cosh a)]/kT}. \quad (2.2)$$

The zero of energy is taken at the energy of the trap, while the trap depth Δ is taken to be the difference in energy between the trap level and the $k=0$ level of the exciton band in the approximation that the wave vector of the radiation field has zero momentum.⁵ This is the depth which can be measured spectroscopically from absorption or emission experiments at low temperatures. The first term in z is simply the Boltzmann factor for the trap level, while the second term is associated with the nondegenerate $k=0$ level of the band. Apart from $k=0$, k can take on values greater than 0 to $\pm\pi/a$, and thus, all non- $(k=0)$ states in the

band are doubly degenerate. If there are $(2N)$ states in the band plus the $k=0$ state, corresponding to $(2N+1)$ molecules in a linear chain, then the final term in the partition function is a summation over N doubly degenerate states, where k takes on values $\pi/aN, 2\pi/aN, 3\pi/aN, \dots, N\pi/aN = \pi/a$. The energy dependence of the band on quantum number k is given by Eq. (2.1), and the partition function has been written so that the $k=0$ level has energy Δ .

In terms of the partition function z the probability that an excitation of the system is in the trap is simply

$$P_{\text{trap}} = 1/z. \quad (2.3)$$

The intensity of emission, I , from the trap is

$$I_{\text{trap}} = K_{\text{trap}}^r N_{\text{trap}}, \quad (2.4)$$

where K_{trap}^r is the radiative rate constant and N_{trap} is the number of trap states populated. If the total number of states excited in the system is N_{tot} , then

$$N_{\text{trap}} = P_{\text{trap}} N_{\text{tot}}, \quad (2.5)$$

and

$$I_{\text{trap}} = K_{\text{trap}}^r N_{\text{tot}} P_{\text{trap}} = K_{\text{trap}}^r N_{\text{tot}} z^{-1}. \quad (2.6)$$

Since K_{trap}^r is essentially temperature independent⁶ and the N_{tot} is usually constant, the temperature dependence of the trap intensity is determined by the temperature dependence of the normalized trap probability $P_{\text{trap}} = z^{-1}$, which includes explicit features of band states.

By varying β and the number of states in the band while keeping the trap depth Δ constant, the relationship between the "real" partition function and a partition function using the degenerate approximation for calculating the trap probability can be seen. Two cases arise, depending upon the sign of β , as illustrated in Fig. 1. If β is negative the exciton band spans an energy range from Δ , the $k=0$ energy, to $\Delta + 4\beta$, the $k = \pm \pi/a$ energy. On the other hand, if β is positive, the band is inverted and it spans an energy range from Δ to $\Delta - 4\beta$. The approximation that all the states in the band are given the energy of the $k=0$ state corresponds to the limiting case of a band with zero bandwidth. In cases where β is finite, however, most states accumulate at the top and bottom of the band, where the density-of-states function for one-dimensional systems⁷ is sharply peaked. One might expect a significant effect on the trap emission owing to the dispersion of the band, particularly when the bandwidth-to-trap-depth ratio $4\beta/\Delta$ takes on reasonable values. Such is indeed the case.

Recently 1, 2, 4, 5-tetrachlorobenzene (TCB) and 1, 4-dibromonaphthalene have been shown to exhibit the properties of one-dimensional excitons. Francis and Harris⁸ measured the bandwidth of

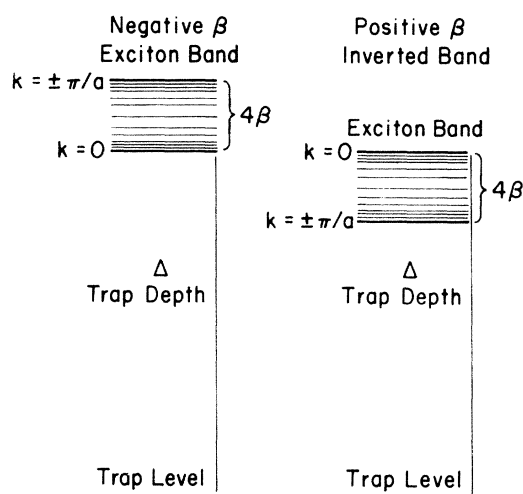


FIG. 1. Trap and exciton energy levels for both negative and positive signs of the intermolecular interaction β . For negative β , the exciton band extends 4β to higher energy than the trap depth Δ , and for positive β the band is inverted and extends 4β to lower energy than Δ .

TCB by an optically detected magnetic-resonance experiment⁹ and found it to be 1.25 cm^{-1} . Hochstrasser and Whiteman¹⁰ in an isotopically-mixed-crystal experiment measured the 1, 4-dibromonaphthalene bandwidth to be 29.6 cm^{-1} . These two values will be used as examples of narrow and broad triplet exciton bands, respectively, although it should be kept in mind that singlet bands can be one or more orders of magnitude greater in width. In Figs. 2(a)–2(e) the trap probability P_{trap} versus temperature is plotted for several different negative values of 4β using the experimental value of Δ (21.3 cm^{-1}) determined for one of the intrinsic traps, hereafter referred to as the X trap in the proto-isotopic crystal $h_2-1, 2, 4, 5$ tetrachlorobenzene (h_2 -TCB).¹¹ In each figure, curves resulting from several different ratios of the number of states in a band to the number of traps are plotted. Figure 2(a) is the degenerate case. Figure 2(b) uses the small value of β taken to be the narrow-band example. Figures 2(c) and 2(d) are calculated using intermediate values, and Fig. 2(e) uses a value associated with a broader band. In Fig. 3, one line from each of the Fig. 2 drawings is shown so that the differences can be more clearly seen. The number of k states (i.e., the number of molecules in the chain) has been kept constant in Fig. 3. Figures 4(a)–4(e) are similar plots; however, a positive sign of β is considered. As illustrated in Fig. 1, as β becomes more negative the energy differences between the trap and all the states in the band, except the $k=0$ state, become greater. For a given number of states the temperature dependence of the trap probability, and therefore the

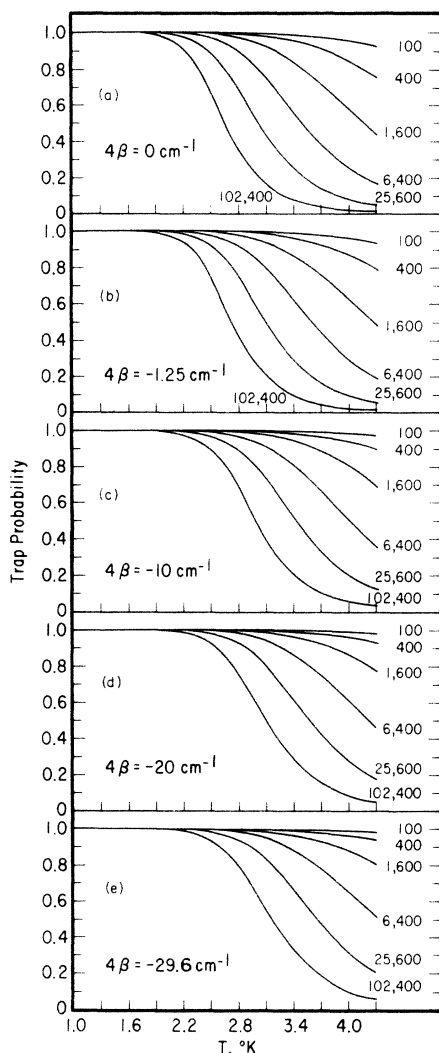


FIG. 2. Calculated trap probabilities, which are proportional to trap intensities, are shown as a function of temperature for various negative values of β . The numbers to the right of each set of curves give the number of exciton k states (number of molecules per chain) per trap state used to calculate the curve. The trap depth Δ used is the tetrachlorobenzene trap depth, 21.3 cm^{-1} . (a) illustrates the limiting case of a band with zero width, $4\beta = 0$. (b) uses the bandwidth previously reported for tetrachlorobenzene (c) and (d) are for intermediate bandwidths, and (e) is calculated using the reported 1, 4-dibromonaphthalene bandwidth. As the bandwidth becomes more negative, the energy differences between the trap and states in the band become greater and the temperature dependence of the trap probability becomes more gradual.

change in emission, is more gradual. As β takes on larger positive values, the energy differences between the states in the band and the trap become smaller. This causes the trap probability (and the trap intensity) to have a steeper temperature dependence. Figure 4(e) is an example where 4β ,

the bandwidth, is greater than Δ , and hence the bottom of the band extends below the trap. When the trap and exciton states become degenerate it is necessary to consider additional perturbations. In particular, a realistic treatment should include the localization of band states by the trap impurity and the delocalization and energy shift of the trap state via interactions with band states.^{12(a)} Furthermore, when the number of impurity states becomes significant relative to the number of band states, amalgamation must be considered in detail.^{12(b)} This would cause a deviation from the zeroth-order temperature dependence illustrated in Fig. 4(e). In Fig. 5 one curve from each of the Fig. 4 drawings is plotted so that the change in the temperature dependence with β can be seen more clearly. One notes that the temperature dependence of trap emission, in addition to being dependent on the trap depth and trap concentration, is significantly governed by the detailed structure of the exciton band. In the case of degenerate trap and band states in the absence of trap-band interactions, for example, a reversal in the temperature dependence results [cf. Fig. 4(e)]. In other cases, each value of the chain length and bandwidth generates a unique temperature dependence in the trap phosphorescence. Indeed, this interrelationship between the bandwidth, exciton chain length, and trap depth can be exploited to give an experimental measure of these parameters in crystals representative of one-dimensional systems. The temperature dependence of trap emission can also be used to determine (via inference) whether or not the band and trap states are in Boltzmann equilibrium. An example of this is illustrated in Fig. 6, where the experimental temperature dependence of the intensity of the intrinsic h_2 -TCB X trap is plotted as a function of temperature. The best calculated fit to the experimental data is also shown along with values of the parameters which are well outside of the limits

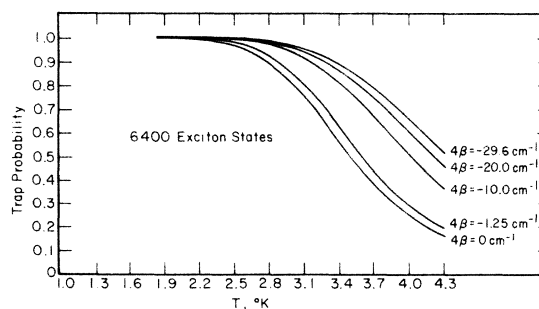


FIG. 3. One curve from each of the five sets of curves of Fig. 2 is displayed so that the temperature dependence of the trap probability as a function of β can be more clearly seen. The curves are for 6400 exciton k states per trap using the negative values of 4β from Fig. 2.

on the accuracy of the results. Since the trap is intrinsic, the trap concentration was unknown; consequently, both β and the trap concentration were varied in order to obtain the calculated curve. The best values are $3.5 \pm 2 \text{ cm}^{-1}$ for the bandwidth 4β , with β positive and a trap concentration of one

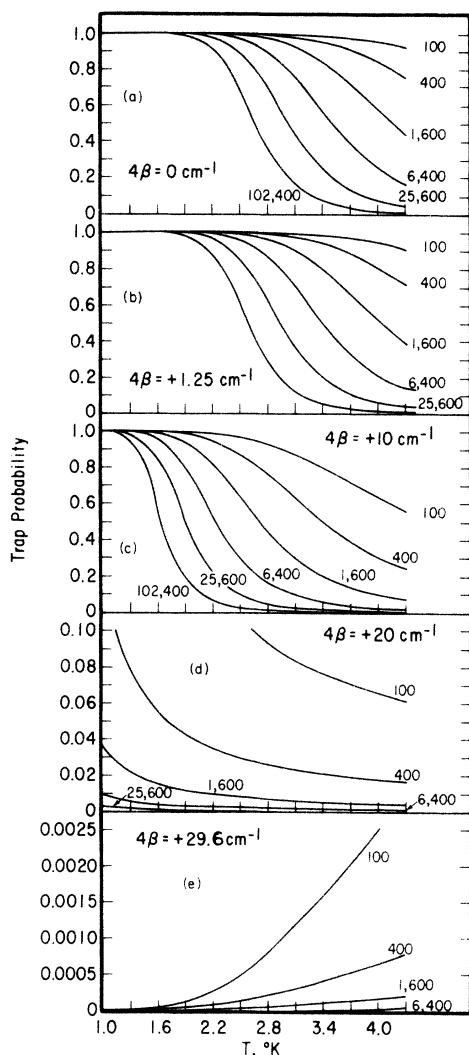


FIG. 4. Calculated trap probabilities, which are proportional to trap intensities, are shown as a function of temperature for various positive values of β . The number next to each curve gives the number of exciton states per trap state. The 21.3-cm^{-1} tetrachlorobenzene trap depth Δ is used. The bandwidth, 4β , used to calculate the curves is given in each section of the drawing. It should be noted that the scale changes in (d) and (e). As the bandwidth 4β becomes increasingly more positive the energy differences between the trap and the levels of the band become smaller, resulting in a steeper temperature dependence of trap probability. (e) is an example of the amalgamation limit, where the bottom of the band extends below the trap depth.

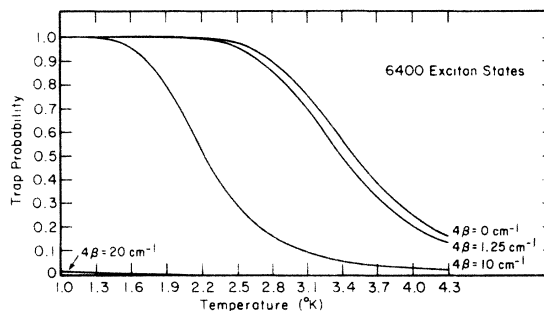


FIG. 5. One curve from each of the sets of curves in Fig. 4(a)–4(d) is displayed so that the temperature dependence of the trap probability as a function of β can be more clearly seen. The curves are for 6400 exciton k states per trap using the positive values of 4β from Fig. 4.

part in 90 000. If the trap concentration is known from an independent measurement, the uncertainty in the bandwidth measured in this type of experiment can be greatly reduced. Although the h_2 -TCB bandwidth measured by this method is somewhat larger than that reported⁸ (1.25 cm^{-1}) from an independent method, the essential features of these results are in agreement with the interpretation of the earlier results. It is important to note that the earlier experiments⁸ and the above experiment can only be fully understood and interpreted in

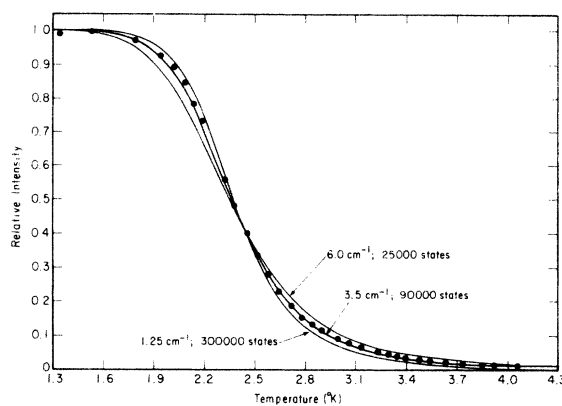


FIG. 6. Solid circles are the experimentally determined intensity-versus-temperature data for the 21.3-cm^{-1} trap in 1, 2, 4, 5-tetrachlorobenzene. The center solid line is the theoretically determined best fit of the data to the bandwidth 4β and the number of exciton k states which corresponds to the number of molecules in the average exciton chain. The two additional curves, labeled 1.25 and 6.0 cm^{-1} , correspond to values well outside the standard deviation of the data and are illustrated to demonstrate the uniqueness of the data in the variables 4β and the number of k states. The best value of the bandwidth is $3.5 \pm 2 \text{ cm}^{-1}$, with β positive.

terms of a model which is dependent upon coherent migration being the principal mode of exciton transport in the TCB crystal at low temperatures. The importance of coherent migration in the above results is discussed in detail in Sec. III. The discussion in this and following sections is primarily concerned with excited triplet states; however, it should be kept in mind that identical considerations also apply to singlets and transport properties in general.

III. EXCITON GROUP VELOCITIES AND THERMAL EQUILIBRIUM

In the Frenkel limit once a molecule is excited it cannot transfer its excitation to another molecule without an intermolecular interaction which destroys the degeneracy of the states. In a finite band, the velocity with which an excitation propagates in the crystal with a particular momentum in a coherent model is the group velocity $V_g(k)$, which is given by the slope of the energy dispersion of the band

$$V_g(k) = \frac{1}{\hbar} \frac{\partial E(k)}{\partial k}, \quad (3.1)$$

and is proportional to the change in exciton energy with k . For a nondegenerate band at nonzero temperatures, the group velocity will be finite because of the population of non- $(k=0)$ or non- $(\pm\pi/a)$ wave-vector states and the excitation will be able to migrate. The average velocity of this migration, and certain details of phonon-exciton scattering, determines whether or not the system can reach thermal equilibrium. If during the lifetime of the excited state the excitations do not travel far enough to reach traps, the trap probability cannot be described by Boltzmann statistics. On the other hand, if the excitations during their lifetime can travel, on the average, many times farther than the average distance between traps, then all the excitations will be able to "sample" traps, the system will be able to reach thermal equilibrium, and the trap probability will be determined by the partition function of Sec. II. The importance of phonon-exciton scattering in the equilibration process cannot be underestimated, for it is what ultimately limits the mean free path of coherent propagation.^{13,14} If we assume that there is no memory between phonon-exciton scattering events and restrict the scattering to stochastic first-order Markoffian processes¹⁵ one can assign a coherence time $\tau(k)$ to the wave packets propagating at velocities $V_g(k)$. The distance $l(k)$ a coherent state propagates between "random" scattering events is then given by

$$l(k) = V_g(k)\tau(k) \quad (3.2)$$

and is thus equivalent to a mean free path.

At intermediate temperatures, where the princi-

pal limitation on $\tau(k)$ is phonon-exciton scattering, Frenkel excitons initially in a state k (or a linear combination of k states) scatter to other k' states in a time short compared to the radiative or radiationless lifetime, but in a time long compared to the intermolecular interaction time (β^{-1}). As a result, the coherence time $\tau(k)$ is shortened, the mean free path is reduced, and the ability to equilibrate trap and exciton states is attenuated. We will show in a later publication that scattering is principally to adjacent k states and hence the average group velocity is relatively unaffected until one approaches the high-temperature limit. Diffusion or random walk is simply the limit where the change in k occurs on a time scale short compared to β^{-1} . These features will be dealt with in far greater detail in a subsequent paper,¹⁶ where a method for observing the dynamics of individual k states will be presented. In the present case, however, only manifestations of the average velocities [and/or $\tau(k)$'s] are easily measurable and therefore we restrict the discussion to these features. The importance of $\langle V_g(T) \rangle$ is easily seen by comparing coherent and incoherent migration.

Treating the exciton band as one dimensional, the average group velocity at a given temperature, $\langle V_g(T) \rangle$, is given by the normalized sum over the velocities of the k states in the band, with each velocity weighted by the probability of finding the system in that k state at a particular temperature T , i. e.,

$$\langle V_g(T) \rangle = \frac{1}{\hbar} \left\langle \frac{\partial E(k)}{\partial k} \right\rangle_T = \frac{2\beta a}{\hbar} \frac{\sum_k \sin(ka) e^{-(2\beta \cos ka/kT)}}{\sum_k e^{-(2\beta \cos ka/kT)}}. \quad (3.3a)$$

We will restrict the summation in (3.3a) to positive wave-vector states only so that $\langle V_g(T) \rangle$ is physically related to a scalar velocity in one direction. In the limit that the number of k states becomes large, the summations in Eq. (3.3a) converge to an integral form which can be evaluated using modified Bessel functions. The resulting expression for the average group velocity is given by

$$\langle V_g(T) \rangle = (2\beta a/\hbar)(2kT/\pi\beta)^{1/2} [I_{1/2}(z)/I_0(z)], \quad (3.3b)$$

where $z = (2\beta/kT)$ and $I_0(z)$ and $I_{1/2}(z)$ are given by

$$I_0(z) = (1/\pi) \int_0^\pi e^{z \cos \theta} d\theta \quad (3.3c)$$

and

$$I_{1/2}(z) = (\frac{1}{2}z/\pi)^{1/2} \int_0^\pi e^{z \cos \theta} \sin \theta d\theta, \quad (3.3d)$$

where $\theta = ka$.

In Table I, group velocities, calculated using Eq. (3.3a), for a narrow, intermediate, and broad triplet band are listed as a function of temperature. The average group velocity is not very sensitive to the number of states in the band when the number of states in the band is greater than 100. It can be

seen from Table I that even for the narrow bandwidth of 1.25 cm^{-1} which Francis and Harris⁸ have reported for TCB, at 1°K an excitation traveling completely coherently will be able to sample 10^9 lattice sites in 10 msec, which is the order of the lifetime of the TCB triplet state.¹¹ (The exciton will of course travel even further given the 3.5-cm^{-1} band reported here.) This is sufficient to enable a system with trap concentrations as low as 1 part per 10^7 to come to thermal equilibrium. For the larger bandwidths, systems with even smaller trap concentrations will be able to equilibrate. Only very pure samples with nearly degenerate bands will be unable to come to thermal equilibrium when the excitons migrate coherently.

Attenuation of this long-range migration occurs when phonon-exciton scattering limits the coherence time and hence the coherence length. When this length becomes less than the average trap-to-trap separation, thermal equilibrium becomes progressively more difficult to achieve. In the high-temperature limit, phonons destroy the translational symmetry of the lattice and tend to scatter an excitation at each lattice site, and hence the group velocity is replaced by a diffusion rate as the excitation executes a random walk at every lattice site. In one-dimensional diffusion, the exciton can move with equal probability to either of the two molecules adjacent to it. The average time τ it takes an exciton undergoing a random-walk migration to take one step is on the order of¹⁷

$$\tau = \hbar/4\beta. \quad (3.4)$$

Hence, the median distance traveled (in cm) is given by

$$\langle d \rangle = \frac{1}{3} N^{1/2} a, \quad (3.5)$$

where N is the number of hops taken per unit time and a is the distance traveled in one hop, one lattice translation (in cm). In Table II the median random-walk distances are listed for the three bandwidths used in Table I for a variety of times. The value of a is 3.76 \AA , which is the translational spacing of molecules along the \bar{a} direction in TCB.¹⁸ Table III also gives the ratio of the distances trav-

TABLE II. Median distance traveled (cm) in a random-walk process.

Time (msec)	Bandwidth		
	1.25 cm^{-1}	15 cm^{-1}	29.6 cm^{-1}
1	7.6×10^{-5}	2.7×10^{-4}	3.7×10^{-4}
10	2.4×10^{-4}	8.4×10^{-4}	1.2×10^{-3}
100	7.6×10^{-4}	2.7×10^{-3}	3.7×10^{-3}
1000	2.4×10^{-3}	8.4×10^{-3}	1.2×10^{-2}

eled by an exciton moving in the coherent limit versus random-walk migration for the three bandwidths at 2.8°K .

It is seen that random-walk migration is a factor of 10^4 to 10^6 slower than coherent migration. While a h_2 -TCB exciton traveling completely coherently could sample approximately 10^9 lattice sites during its lifetime (10 msec), an exciton undergoing random-walk migration on the average will only sample about 10^4 lattice sites. The number of excitons able to migrate larger distance falls off very rapidly because one-dimensional random-walk processes are describable by a Gaussian distribution of distances around some initial starting point.¹⁹ In the case of h_2 -TCB only 3 excitons out of 1000 traveling completely by random-walk migration would be able to cover a distance of 5×10^4 lattice sites, which is half the average distance between traps in these crystals. The obvious conclusion to be drawn is that the observation that the temperature dependence of the h_2 -TCB trap intensity obeys Boltzmann statistics provides strong evidence for coherent migration as the principal mode of exciton transport at liquid-helium temperatures. Indeed the coherence time must be at least several orders of magnitude longer than the intermolecular exchange time in order for the system to achieve thermal equilibrium within the excited-state lifetime.

IV. EFFECTS OF MULTIPLE BANDS

A. Zero-field splitting of the exciton band and trap states

To this point, the triplet exciton band and trap have each been considered as consisting of a single

TABLE I. Average group velocities (cm/sec) for a band of 25 000 k states as a function of temperature.

T ($^\circ \text{K}$)	Bandwidth		
	1.25 cm^{-1}	15 cm^{-1}	29.6 cm^{-1}
1.0	2652	12 747	18 075
1.6	2750	15 996	22 781
2.2	2782	18 592	26 611
2.8	2797	20 762	29 902
3.4	2804	22 601	32 814
4.0	2809	24 161	35 436

TABLE III. Ratio of the coherent migration distance to the random-walk distance at 2.8°K .

Time (msec)	Bandwidth		
	1.25 cm^{-1}	15 cm^{-1} ^a	29.6 cm^{-1} ^a
1	3.7×10^4	7.8×10^4	7.8×10^4
10	1.1×10^5	2.5×10^5	2.5×10^5
100	3.7×10^5	7.8×10^5	7.8×10^5
1000	1.1×10^6	2.5×10^6	2.5×10^6

^aDifferences between the 15 and 29.6 cm^{-1} ratios are less than 1% because of insufficient population in k states at the center of the band at this low temperature.

magnetic sublevel. This is an accurate description for singlet states, but both the triplet exciton band and trap are split into three energy sublevels by the zero-field spin dipolar interaction of the unpaired triplet-electron spins.²⁰ The intensity of trap emission I_{trap} for the three-level system is given by

$$I_{\text{trap}} = K_{x \text{ trap}}^r N_{x \text{ trap}} + K_{y \text{ trap}}^r N_{y \text{ trap}} + K_{z \text{ trap}}^r N_{z \text{ trap}}, \quad (4.1)$$

where $K_{i \text{ trap}}^r$ is the radiative rate constant for the i th sublevel and $N_{i \text{ trap}}$ is the population of the i th sublevel. In the absence of spin-lattice relaxation processes in the band states, the trap states, and between trap and band states, the population of a triplet sublevel is independent of the populations of the other sublevels, and hence the total population of a particular magnetic spin component is the sum of the populations in the particular spin sublevel of the exciton band and the trap. Thus, the trap population of the i th sublevel can be given by

$$N_{i \text{ trap}} = N_{i \text{ tot}} / z_i, \quad (4.2)$$

where z_i is the partition function for the i th-spin sublevel. Under these conditions the total trap intensity can be written as

$$I_{\text{trap}} = K_{x \text{ trap}}^r N_{x \text{ tot}} / z_x + K_{y \text{ trap}}^r N_{y \text{ tot}} / z_y + K_{z \text{ trap}}^r N_{z \text{ tot}} / z_z. \quad (4.3)$$

In the absence of spin-orbit coupling the dispersion of each of the three triplet bands will be identical when the zero-field spin dipole interaction is much smaller than the band dispersion. Thus, the three spin sublevel partition functions, z_x , z_y , and z_z , are essentially the same and the trap intensity is given by

$$I_{\text{trap}} = (K_{x \text{ trap}}^r N_{x \text{ tot}} + K_{y \text{ trap}}^r N_{y \text{ tot}} + K_{z \text{ trap}}^r N_{z \text{ tot}}) / z. \quad (4.4)$$

The net result is that the temperature dependence, as in the single-spin-sublevel case, is determined only by the change in z with temperature.

In general, however, spin-orbit coupling must occur in order to give allowed transition character from the triplet excited state to the ground-singlet manifold.²¹ In most cases the spin eigenfunctions have different symmetry properties resulting in admixture of different singlet states into three individual spin sublevels.²² The dispersion of the three triplet-spin-sublevel bands can differ in such cases, giving each sublevel a slightly different partition function and, therefore, in principle, a different intensity temperature dependence. However, the changes in the dispersions of the bands owing to spin-orbit coupling are, in almost all cases, so small that the temperature dependence

of the intensity of trap phosphorescence is unaffected by these small energy differences. In h_2 -TCB spin-orbit coupling produces only one part in 10^6 difference in the dispersion of the three spin-sublevel bands.⁸

A more serious consideration for molecular systems in some temperature regions is the effect of spin-lattice relaxation on the temperature dependence of trap emission. In the above discussions the steady-state population in the band and trap, N_{tot} , in a particular magnetic sublevel was assumed to be independent of temperature and independent of the populations of the other two sublevels. However, spin-lattice relaxation couples the sublevels, allowing population to be transferred from one to another. Since this is, in general, highly temperature dependent,²³ the total steady-state population of a particular magnetic sublevel can change significantly with temperature. To account for these variations is in principle straightforward. The population of a trap, and therefore its intensity, at any one temperature is determined by the partition function, as before, but as the temperature changes, the change (via T_1) in the total sublevel population as well as the change in the partition function must be determined. The change in the total sublevel populations can be determined by measuring the change in the lifetimes of the three sublevels as a function of temperature, and thereby assessing the amount of spin-lattice relaxation.²⁴ The trap probability is determined, as before, using the partition function, but now it must be multiplied by the relative sublevel population for each temperature, i. e.,

$$I_{\text{trap}} = \left[\sum_{i=x,y,z} K_{i \text{ trap}}^r N_{i \text{ tot}}(T) \right] / z. \quad (4.5)$$

Although the effects of spin-lattice relaxation between the magnetic sublevels of the triplet band in one-dimensional bands can complicate the evaluation of the trap phosphorescence intensity, in most crystals this does not present any real difficulty. It is only when there is a significant temperature dependence of the *effective* spin-lattice relaxation process over the temperature range of interest that difficulty arises. Usually, small two-dimensional exchange interactions between translationally inequivalent molecules in the unit cell result in an effective averaging of the spin-sublevel populations in band states in a time short compared to the lifetime of the state. Thus, the exciton dynamics keep the *individual spin sublevels* close to Boltzmann equilibria, and hence the temperature dependence of spin-lattice relaxation is ineffective in causing large deviations in the individual spin-sublevel populations over the range of temperature of interest. This is the case, at least, for h_2 -TCB and d_2 -TCB, between 1–4 °K.

B. Two- and three-dimensional bands

The above considerations can be readily extended to systems in which a trap interacts with a multi-dimensional exciton band. For one molecule per unit cell the most general form is given by the three-dimensional partition function z :

$$z = 1 + \sum_{k_a=0}^{\pi/a} \sum_{k_b=0}^{\pi/a} \sum_{k_c=0}^{\pi/a} G(k) \exp\{-[\Delta - 2\beta_a(1 - \cos k_a a) - 2\beta_b(1 - \cos k_b b) - 2\beta_c(1 - \cos k_c c)]/kT\}, \quad (4.6)$$

where k_a , k_b , and k_c are the wave vectors associated with the crystallographic translation directions \bar{a} ,

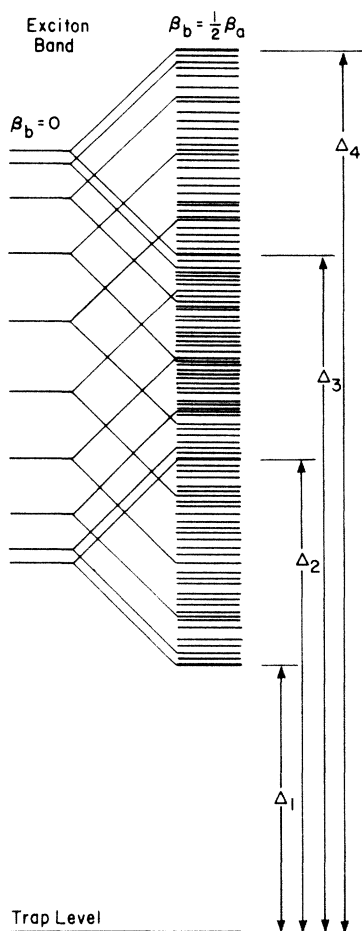


FIG. 7. Trap and exciton energy-level diagrams for a one-dimensional exciton bandwidth $\beta_b = 0$ and a two-dimensional band with $\beta_b = \frac{1}{2}\beta_a$. The spectroscopically determinable trap depth is the difference in energy between the trap level and the $k_a = 0$, $k_b = 0$ level of the two-dimensional exciton band. The trap depth can have one of the four possible values Δ_1 to Δ_4 shown in the figure, depending upon the signs of β_a and β_b . If both β_a and β_b are negative, Δ_1 will be observed. If $\beta_a < 0$ and $\beta_b > 0$, Δ_2 will be observed. If $\beta_a > 0$ and $\beta_b < 0$, Δ_3 will be observed, and if β_a and β_b are both positive, Δ_4 will be the spectroscopically measured value of the trap depth.

\bar{b} , and \bar{c} , and β_a , β_b , and β_c are the nearest-neighbor intermolecular interaction matrix elements along these three axes. $G(k)$ is a degeneracy factor which takes on the value 1 when the value of all three k wave vectors are zero, 2 when any two k wave vectors are zero, 4 when only one k wave vector is zero and, finally, 8 when all three k wave vectors are greater than zero. The partition function for the case in which the exciton band is two dimensional is obtained by setting β_c equal to zero, and the one-dimensional partition function given in Eq. (2.2) follows naturally from Eq. (4.6) by setting β_c and β_b equal to zero.

To simplify the discussion, only the two-dimensional case will be explicitly considered. For illustration β_b is set equal to $\frac{1}{2}$ of β_a and the two-dimensional exciton band is limited to 400 states corresponding to a square array of 400 molecules. An energy-level diagram for the trap and exciton system is given in Fig. 7. As in the one-dimensional case, the 0-0 absorption must obey the selection rule $\Delta k = 0$; thus, the 0-0 transition is associated with the $k_a = 0$, $k_b = 0$ level. Depending upon the signs of β_a and β_b , the $k_a = 0$, $k_b = 0$ exciton level can occur at four different energies relative to the trap energy. As indicated in Fig. 7, if β_a and β_b are both negative, Δ_1 will be the observed trap depth. If β_a is negative and β_b is positive, Δ_2 will be the trap depth. If β_c is positive and β_b is negative, Δ_3 will be the trap depth. If both β_a and β_b are positive, Δ_4 will be the spectroscopically measured trap depth.

For a given trap concentration, the average number of states in the exciton band is known, the trap depth Δ can be measured, and the temperature dependence of the trap intensity can be fit by varying the signs and magnitudes of β_a and β_b in the multidimensional partition function [Eq. (4.6)]. For systems in which the number of states in the band is large, i. e., low trap concentration, the density of states in the band becomes so large that the partition function is not sensitive to β_a and β_b separately but depends only upon the total bandwidth, $4|\beta_a| + 4|\beta_b|$; thus, a measure of the bandwidth can be experimentally determined, even in multidimensional crystals, but details of the band along specific crystallographic axes are lost. The above discussion has been restricted to systems containing trap levels of only one energy. Systems with two or more traps of different energies present a different problem but provide additional and unique information on the exciton dynamics and will be considered in detail below.

V. BOLTZMANN EQUILIBRIA BETWEEN EXCITON STATES AND MULTIPLE TRAPS

The extension of the above treatment to systems in which there are two or more types of traps

having different energies would be straightforward if it were not for the fact that the excitons and traps have finite lifetimes. If the excited-state lifetimes were long enough, the system would come to thermal equilibrium at any temperature and a statistical treatment would always be proper for any temperature or trap depth. However, given the finite lifetimes of the states involved, a statistical approach is only possible above a certain characteristic temperature, hereafter termed T_c , which is determined by the trap depths, the trap concentration, and the exciton bandwidth.

The inability of the system to achieve thermal equilibrium below the characteristic temperature is due in part to the spacial separation of the traps of different energies and in part to different trap-phonon interactions at the different trap sites in the lattice. This can be seen more clearly by considering the energy-level diagram in Fig. 8 for a system consisting of an exciton band, a shallow trap τ_s , and a deep trap τ_d . The dashed arrows indicate the possible paths electronic excitations can travel in the system in the absence of direct long-range energy exchange between traps. Basically, an excitation cannot be transferred to another trap site without first being thermally promoted to the exciton band in which it can migrate to another trap site and again be trapped. Equilibrium is only established through a continuous process of detrapping, migration, and retrapping. If the process continues long enough, the system reaches its equilibrium population distribution in spite of the fact that the shallow and deep traps exchange their population with the band states at different rates. Because the exciton and trap states have a finite lifetime, however, the rate of detrapping and re-

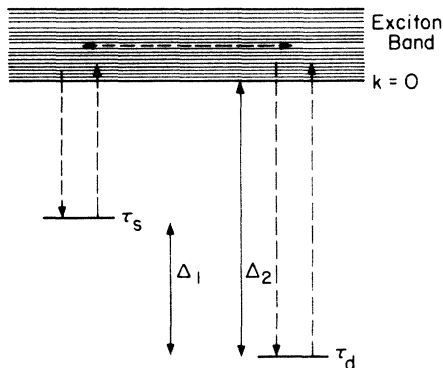


FIG. 8. Energy-level diagram for a system containing an exciton band and traps of two different energies. τ_s labels the shallow traps, and τ_d labels the deep traps. Δ_1 is the energy difference between τ_s and τ_d , and Δ_2 is the energy difference between τ_d and the $k=0$ level of the exciton band. The dashed arrows indicate the possible paths an excitation can travel in the system.

trapping for both traps must be large enough to compete with radiative and radiationless processes. This can only occur above some characteristic temperature T_c , where phonon-trap interactions are frequent enough to keep the system in thermal equilibrium.

In the equilibrium temperature region, the temperature dependence of the trap intensities can be determined from the probabilities P_{τ_d} and P_{τ_s} that an excitation will be in deep trap τ_d or shallow trap τ_s , respectively. Taking the exciton band to be one-dimensional in the nearest-neighbor approximation, the partition function z for the system is given by

$$z = 1 + G_1 e^{-\Delta_1/kT} + G_2 e^{-\Delta_2/kT} + \sum_{k=\pi/na}^{(n-1)\pi/na} 2G_2 e^{-[\Delta_2 - 2\beta(1 - \cos ka)]/kT}. \quad (5.1)$$

The zero of energy is taken as the energy of the deep trap. As shown in Fig. 8, Δ_1 is the energy difference between the deep and shallow traps, and Δ_2 is the energy difference between the deep trap and the $k=0$ level of the exciton band. The $k=0$ level may be at the top or bottom of the band (as discussed previously) depending upon the sign of β . The concentration of the traps and excitons are normalized to a unit concentration of the deep trap. The first term in z is due to the deep trap. The second term is the Boltzmann factor for the shallow trap multiplied by G_1 , the number of shallow traps relative to a single deep trap. The third term is the Boltzmann factor for the nondegenerate $k=0$ level of the exciton band times G_2 , the number of exciton chains relative to a single deep trap. The final summation is over the remainder of the exciton k states, which are doubly degenerate, giving rise to the factor of 2. The total number of host molecules relative to one deep trap is $G_2(2n)$, where there are $2n$ states per exciton and G_2 exciton chains per deep trap. The trap probabilities P_{τ_d} and P_{τ_s} (which are proportional to the trap intensities) are

$$P_{\tau_d}(T) = 1/z(T) \quad (5.2)$$

and

$$P_{\tau_s}(T) = G_1 e^{-\Delta_1/kT} / z(T), \quad (5.3)$$

respectively. Calculated plots of P_{τ_d} and P_{τ_s} versus temperature for systems which contain 99.2% host-exciton states, ~0.8% shallow traps, and 1.6×10^{-30} deep traps are illustrated in Fig. 9. The trap depths Δ_1 and Δ_2 are 10 and 20 cm^{-1} , respectively. These values are typical of singly and doubly protonated traps in deuterio crystals. The curves are for a range of bandwidths, 4β , between +8 and -8 cm^{-1} . Several features of the trap phosphorescence intensity in multiple-trap systems are particularly noteworthy. First, as 4β

becomes more positive the energy levels in the band become closer to the trap levels. This results in a loss of trap probability and therefore a loss of trap intensity. Although both traps are affected, the changes in the deep- and shallow-trap probabilities are entirely different. The decrease in the deep trap phosphorescence with increasing temperature results from the partitioning of the excitation into the higher-energy shallow trap and exciton states. When the number of molecules in an exciton chain (the number of k states in the band) greatly exceeds the number of shallow traps, the form of the deep-trap temperature dependence becomes indistinguishable from the single-trap problem considered earlier. The temperature dependence of the shallow trap is not so simple. Physically, as the temperature increases from a value where only the deep trap is emitting ($P_{\tau_d} = 1.0$, $P_{\tau_s} = 0.0$), the initial loss in τ_d results in the onset of τ_s emission. How rapidly τ_s increases with increasing temperature, however, is determined by the partitioning of energy from the shallow trap into the band states. If many exciton states are near in energy to the shallow trap, the shallow trap will never acquire a significant intensity because of the ability of the exciton states to partition the energy, i. e., large value of the band partition function. This occurs when the shallow-trap depth ($\Delta_2 - \Delta_1$ in Fig. 8) is small and/or the exciton band has a large number of k states at energies near the shallow trap (positive β). On the other hand, when the shallow-trap depth becomes larger and/or the

exciton band has a smaller positive dispersion or negative dispersion, the shallow-trap emission will continue to increase in intensity at the expense of the deep-trap probability until a point when the Boltzmann factor starts to significantly populate the exciton state. At this point the shallow trap will lose intensity with increasing temperature because of partitioning to the band. An important point of the temperature variation of both the deep and shallow traps is that for every curve associated with the deep trap there is a unique shallow-trap curve for a specific value of the band dispersion, number of k states, and number of shallow traps. Moreover, the detailed shape of the temperature-dependence curve for the shallow traps is determined by the partition function. A variation in τ_d and τ_s trap emission as a function of concentration is illustrated in Fig. 10. The value of the band dispersion and trap depth have been fixed at $4\beta = 4 \text{ cm}^{-1}$, $\Delta_1 = 10 \text{ cm}^{-1}$, and $\Delta_2 = 20 \text{ cm}^{-1}$. As is expected, when the shallow-trap concentration increases relative to the band states the intensity peaks at higher temperatures. The values plotted in Fig. 10 are representative of mixed crystals, where the band states are the pure deuterio (d_2) isotope (2 deuteriums/molecule), the shallow trap is the hd isotope, and the deep trap is the h_2 molecule. The concentration values listed for cases A through D correspond to statistical mixtures of the various species based upon the total deuterium concentration of the crystals.

The practical use of such an approach to obtain

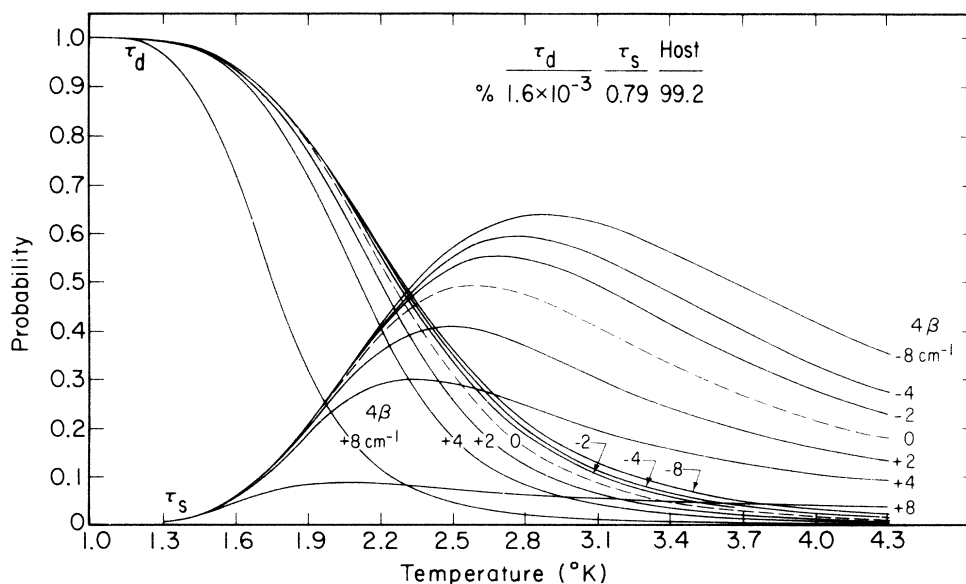


FIG. 9. Trap probabilities, which are proportional to phosphorescence intensities, as a function of temperature are plotted for an exciton and a two-trap-type system. τ_s and τ_d are 10 and 20 cm^{-1} below the $k=0$ level of the band, respectively. Each pair of lines, one for τ_d and one for τ_s , is calculated using the indicated exciton bandwidth, 4β . The percent of each of the species is given at the top of the figure.

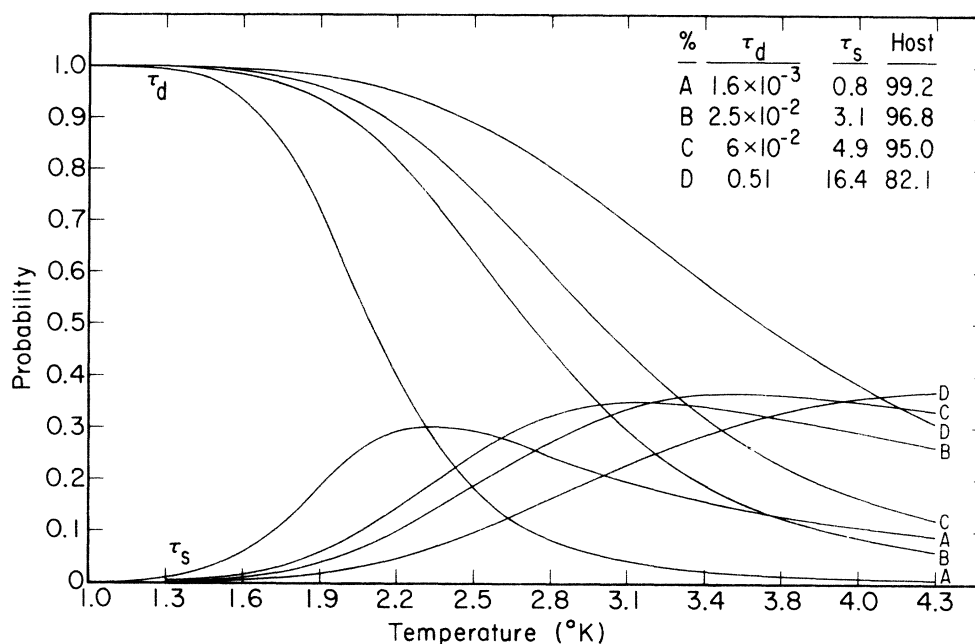


FIG. 10. Trap probabilities as a function of temperature for different percent compositions of the three species in the crystal indicated at the top of the figure. The two traps have 10- and 20-cm⁻¹ trap depths and the exciton bandwidth is 4 cm⁻¹ for all curves.

information about the band is straightforward and self-evident. If a sample is prepared with two traps of known concentration, where Δ_1 and Δ_2 can be measured spectroscopically, then the band dispersion and the sign of β can be determined from the temperature dependence of the two trap intensities. Figure 11 illustrates this for deuterio-proto mixed crystals of TCB. Figure 11(a) is the temperature dependence of h_2 -TCB(τ_d) and hd -TCB(τ_s) trap phosphorescence in a d_2 -TCB crystal in the temperature range 1.3 to 3.8 °K. Details of the preparation and characterization of the traps are given in Sec. VIII. The data illustrate two distinct temperature regions, one below and one above a characteristic temperature T_c . These are labeled I and II, respectively, and correspond to regions where Boltzmann statistics are appropriate (II) because the trap and band state are in thermal equilibria, and where Boltzmann statistics are inappropriate (I) because the finite lifetime of the excited states are short relative to the time necessary to equilibrate both the deep and shallow traps with the exciton band states.

Using the experimental values for Δ_1 , Δ_2 , τ_s , and τ_d , an excellent fit for both the deep- and shallow-trap temperature dependence in region II is simultaneously obtained for the lowest triplet band in d_2 -TCB. A total bandwidth of 12 ± 2 cm⁻¹ and a positive intermolecular exchange interaction for d_2 -TCB from these experiments (cf. Fig. 11) is to

be compared to a total bandwidth of 3.5 cm⁻¹ and a positive intermolecular exchange interaction for the same band in h_2 -TCB (cf. Fig. 6). The relationships between isotope effect, the Born-Oppenheimer approximation, and the band dispersion in these crystals will be discussed in a later publication.²⁵

In the remainder of this paper we will discuss the non-Boltzmann region (I) and formulate a general approach to exciton dynamics in this region which is amenable to experimentation. This region is characterized by insufficient phonon-trap interaction to provide thermal equilibrium between trap and band states. We will defer detailed interpretation of TCB in this region until later, but we will demonstrate proof that TCB in this region is not in thermal equilibrium but characterized by considerations of Sec. VI.

VI. NON-BOLTZMANN DISTRIBUTIONS BETWEEN EXCITON AND TRAP STATES

Below a characteristic temperature, the system does not come to thermal equilibrium within the lifetimes of the states because the phonon interaction with the trap states does not equilibrate the trap and band states at a fast enough rate. The problem must therefore be treated in terms of a set of coupled rate equations for the processes which are occurring. Differential equations describing the time variation of the states illustrated

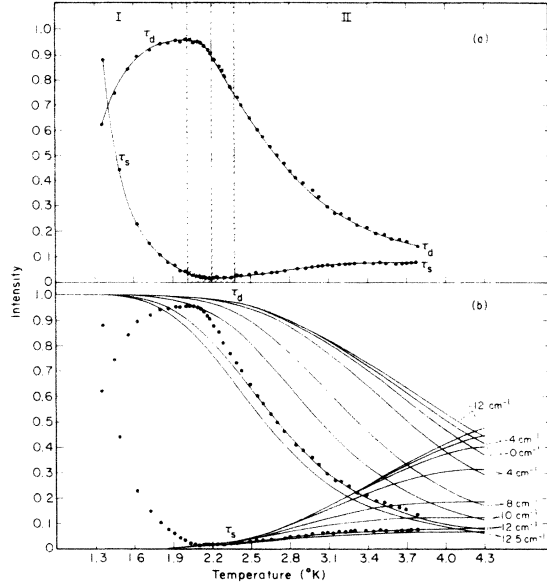


FIG. 11. (a) displays the intensity-versus-temperature experimental data. The deep trap τ_d is h_2 -TCB, the shallow trap τ_s is h_d -TCB, and the host molecules which comprise the exciton chains are d_2 -TCB. The shallow- and deep-trap depths are, respectively, 12.8 and 23.5 cm^{-1} . Region I is the non-Boltzmann temperature region, and region II is the temperature region in which the system is in thermal equilibrium. The shaded section indicates the transition region. (b) shows the experimental data in addition to curves calculated for various exciton bandwidths, 4β , using the experimental trap depths and trap concentrations. It can be seen that in the Boltzmann equilibrium region II, both the shallow-trap data and the deep-trap data fall on the 12- cm^{-1} shallow- and deep-trap calculated curves.

in Fig. 12 are given in Eqs. (6.1)–(6.4):

$$\frac{d[E]}{dt} = K^{\text{ISC}}[S^1] + K_{d0}[\tau_d] + K_{s0}[\tau_s] - K_{d1}[E] - K_{s1}[E] - K_E[E], \quad (6.1)$$

$$\frac{d[\tau_d]}{dt} = K_{d1}[E] - K_{d0}[\tau_d] - K_d[\tau_d], \quad (6.2)$$

$$\frac{d[\tau_s]}{dt} = K_{s1}[E] - K_{s0}[\tau_s] - K_s[\tau_s], \quad (6.3)$$

$$\frac{d[S^1]}{dt} = P[S^0] - K_{s1}[S^1] - K^{\text{ISC}}[S^1]. \quad (6.4)$$

$[E]$ is the exciton population; $[S^1]$ is the population of the first excited singlet band, and $[S^0]$ is the ground-state concentration; $[\tau_d]$ and $[\tau_s]$ are the deep- and shallow-trap populations; P is the rate constant for the production of excited singlet excitons, and K_{s1} is the rate constant for the relaxation of singlets to the ground-state manifold S^0 , while K^{ISC} is the intersystem crossing rate con-

stant. K_E , K_d , and K_s are the total rate constants for relaxation to the ground state from the exciton bands, deep traps, and shallow traps, respectively; they include radiative and radiationless processes. K_{s1} and K_{d1} are the trapping rate constants for excitons entering the shallow and deep traps, respectively, and K_{s0} and K_{d0} are the detrapping rate constants of the shallow and deep traps into the exciton bands. Implicit in the kinetic equations is the assumption that the excited-state concentrations are low enough to ensure that bimolecular annihilation and other nonlinear effects may be neglected. The ground-state concentration $[S^0]$ is taken as a constant. If the lifetimes of the excited states are short, then $[S^0]$ will be the concentration of host molecules in the crystal. If the lifetimes of the exciton and trap states are long but are approximately the same, $[S^0]$ will remain constant with changing temperature since transferring population between excited states of the same lifetime will not result in changing $[S^0]$. However, if the lifetimes are long and differ greatly, then $[S^0]$ can change with temperature but will still be constant at any one temperature. Hence, Eqs. (6.1)–(6.4) can be solved for $[\tau_s]$ and $[\tau_d]$ by assuming steady state. The results are

$$[\tau_s] = \frac{AK_{s1}(K_d + K_{d0})}{(K_d + K_{d0})(K_s + K_{s0} - CK_{s1}) - BK_{d1}(K_s + K_{s0})} \quad (6.5)$$

and

$$[\tau_d] = \frac{AK_{d1}(K_s + K_{s0})}{(K_d + K_{d0})(K_s + K_{s0} - CK_{s1}) - BK_{d1}(K_s + K_{s0})}, \quad (6.6)$$

where

$$A = \frac{PK^{\text{ISC}}[S^0]}{(K_{s1} + K^{\text{ISC}})(K_E + K_{d1} + K_{s1})}, \quad (6.7)$$

$$B = \frac{K_{d0}}{(K_E + K_{d1} + K_{s1})}, \quad (6.8)$$

$$C = \frac{K_{s0}}{(K_E + K_{d1} + K_{s1})}. \quad (6.9)$$

A. Non-Boltzmann low-temperature limit

At some temperature well below the characteristic temperature T_c , K_{s0} and K_{d0} will become insignificant because of the lack of phonons to equilibrate the trap and band states at a rate comparable to the lifetime. Setting these two constants equal to zero in Eqs. (6.5) and (6.6) yields a low-temperature limit for τ_d and τ_s given by

$$[\tau_d] = AK_{d1}K_d^{-1}, \quad (6.10a)$$

$$[\tau_s] = AK_{s1}K_s^{-1}, \quad (6.10b)$$

where the constants K_d^{-1} and K_s^{-1} are the deep- and shallow-trap lifetimes. K_{d1} and K_{s1} , the rate constants for excitons flowing into the traps, can be identified in the coherent model with the average

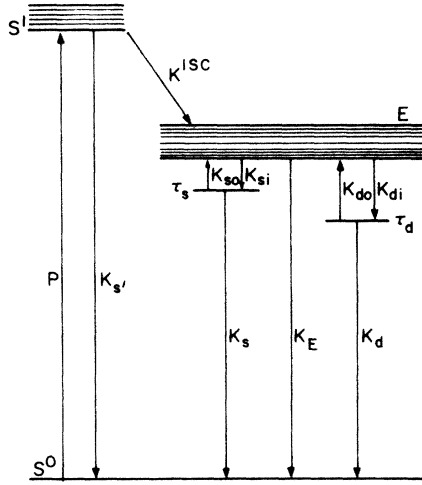


FIG. 12. Energy-level diagram for an exciton and two-trap system showing rate constants used in the non-Boltzmann temperature region. K_s , K_E , K_d , and K_{s1} are the total rate constants for relaxation to the ground state S^0 for the shallow trap τ_s , the exciton band E , the deep trap τ_d , and the first excited singlet state S^1 , respectively. P is the rate constant for the production of excited singlet states and K^{ISC} is the intersystem crossing rate constant. K_{s1} and K_{d1} are the rate constants for excitations flowing into the shallow and deep traps, respectively, and K_{s0} and K_{d0} are the rate constants for excitations flowing out of the shallow and deep traps, respectively.

group velocity of the excitons, $\langle V_g \rangle$, weighted by the distance between traps, i. e.,

$$K_{d1} = \langle V_g \rangle d_d^{-1}, \quad (6.11a)$$

$$K_{s1} = \langle V_g \rangle d_s^{-1}. \quad (6.11b)$$

The average exciton group velocity at a particular temperature is given by Eq. (3.3a), and d_d and d_s are the average distances between the deep- and shallow-trap sites, respectively. It should be noted, however, that the relationship between K_{d1} , K_{s1} , and $\langle V_g \rangle$ need not be restricted solely to coherent migration. The effects of phonon-exciton or impurity-exciton scattering on the average group velocities could be incorporated into K_{d1} and K_{s1} in cases intermediate between pure coherent migration and random-walk migration when the explicit k dependence of these processes are delineated. In the limit that all coherence is lost via these interactions, the average group velocity approaches a temperature-independent velocity given by the random-walk parameters τ and $\langle d \rangle$ of Eqs. (3.4) and (3.5), respectively, i. e.,

$$\langle V_g \rangle \rightarrow \langle d \rangle / \tau. \quad (6.11c)$$

Furthermore, the attenuated velocities in the intermediate- and high-temperature limits could be substituted into the above equations [(6.11a) and

(6.11b)] and a kinetic description of energy migration in these limits would be given by substituting the appropriate velocity in the following equations. The trapping rate constants K_{d1} and K_{s1} are the inverse of the average time it takes an exciton to reach a trap, and hence, in the temperature region under consideration, the rate of finding the trap is inversely proportional to the number of trapping sites available. The concentration of populated deep and shallow traps is then simply given by

$$[\tau_s] = A \langle V_g \rangle K_s^{-1} d_s^{-1}, \quad (6.12a)$$

$$[\tau_d] = A \langle V_g \rangle K_d^{-1} d_d^{-1}, \quad (6.12b)$$

or

$$[\tau_s] = A \langle V_g \rangle K_s^{-1} N_s, \quad (6.13a)$$

$$[\tau_d] = A \langle V_g \rangle K_d^{-1} N_d, \quad (6.13b)$$

where N_d and N_s are the deep- and shallow-trap site concentrations. When the rate of trapping is large relative to the decay of the exciton through other channels ($K_{d1} + K_{s1} \gg K_E$), the steady-state trap concentrations become independent of the average group velocity associated with exciton migration and hence independent of temperature:

$$[\tau_s] \approx \left(\frac{PK^{ISC}}{K_{s1} + K^{ISC}} \right) (K_s^{-1}) \left(\frac{N_s}{N_s + N_d} \right) [S_0] \quad (6.14a)$$

and

$$[\tau_d] \approx \left(\frac{PK^{ISC}}{K_{s1} + K^{ISC}} \right) (K_d^{-1}) \left(\frac{N_d}{N_d + N_s} \right) [S_0], \quad (6.14b)$$

and the ratio of the steady-state concentrations is simply proportional to their respective total concentrations:

$$\frac{[\tau_s]}{[\tau_d]} = \frac{K_s^{-1} N_s}{K_d^{-1} N_d}. \quad (6.15)$$

On the other hand, when the exciton decay competes with or is greater than the rate of trapping ($K_E \gg K_{s1} + K_{d1}$), the steady-state trap concentrations are proportional to the temperature-dependent average group velocity of exciton wave packets and are given by

$$[\tau_s] = \left[\frac{PK^{ISC}[S_0]}{(K_{s1} + K^{ISC})K_E} \right] \langle V_g \rangle K_s^{-1} N_s \quad (6.16a)$$

and

$$[\tau_d] = \left[\frac{PK^{ISC}[S_0]}{(K_{s1} + K^{ISC})K_E} \right] \langle V_g \rangle K_d^{-1} N_d. \quad (6.16b)$$

The ratio of concentrations, however, still remains velocity and therefore temperature independent and is also given by Eq. (6.15).

Since the intensity of emission from the traps is proportional to number of trap sites, the invariance of the ratio over a finite temperature range provides an experimental test of this limit. In addi-

tion, since the temperature dependences of $[\tau_s]$ and $[\tau_d]$ result from a change in the average group velocity, the trap emission provides a tool capable of investigating the average velocity distribution in the exciton band and hence the coherence even at the very lowest temperatures.

B. Non-Boltzmann intermediate temperatures

As the temperature is increased toward T_c , the rate constants for energy transferring from traps to exciton bands are expected to increase. However, if the depths of the traps τ_s and τ_d below the bottom of the band are significantly different relative to kT , then excitations will be able to thermalize from the shallow trap τ_s into the band at temperatures too low for excitations to thermalize from τ_d . The net result is that K_{so} will become significant at temperatures where K_{do} is still negligible. Setting K_{do} equal to zero in Eqs. (6.5) and (6.6), the concentration of traps is given by

$$[\tau_s] = AK_{si} \left[K_s + \left(1 - \frac{K_{si}}{K_E + K_{di} + K_{si}} \right) K_{so} \right]^{-1}, \quad (6.17a)$$

$$[\tau_d] = AK_{di}(K_s + K_{so}) \left\{ K_d \left[K_s + \left(1 - \frac{K_{si}}{K_E + K_{di} + K_{si}} \right) K_{so} \right] \right\}^{-1}. \quad (6.17b)$$

The dependence of these equations on $\langle V_g \rangle$ can be seen by substituting (6.11a) and (6.11b) for K_{di} and K_{si} . In this region the temperature dependence of τ_s and τ_d results from both the temperature dependence of $\langle V_g \rangle$ and the shallow detrapping rate constant K_{so} . Specifically, when the radiative and radiationless decay of the exciton states to the ground state is slow relative to trapping, $K_E \ll K_{di} + K_{si}$, the group-velocity dependence contained in K_{di} and K_{si} vanishes and τ_s and τ_d are given by

$$[\tau_s] = \left(\frac{PK^{\text{ISC}}[S_0]}{K_{s1} + K^{\text{ISC}}} \right) \left(\frac{N_s}{N_d + N_s} \right) \times \left\{ K_s + \left[1 - \left(\frac{N_s}{N_s + N_d} \right) K_{so} \right] \right\}^{-1} \quad (6.18a)$$

and

$$[\tau_d] = \left(\frac{PK^{\text{ISC}}[S_0]}{K_{s1} + K^{\text{ISC}}} \right) \left(\frac{K_s + K_{so}}{K_d} \right) \left(\frac{N_d}{N_d + N_s} \right) \times \left\{ K_s + \left[1 - \left(\frac{N_s}{N_d + N_s} \right) K_{so} \right] \right\}^{-1}, \quad (6.18b)$$

respectively. Hence, the only temperature dependence of τ_s and τ_d is contained in K_{so} . In the other limit, when trapping is slow relative to the radiative and radiationless decay of the exciton states, $K_E \gg K_{di} + K_{si}$, the shallow-trap population reflects the average group velocity of the excitons via its trapping rate from the band (K_{si}); i. e.,

$$[\tau_s] = \frac{PK^{\text{ISC}}[S_0]}{(K_{s1} + K^{\text{ISC}})(K_E)} \left(\frac{K_{si}}{K_s + K_{so}} \right). \quad (6.19a)$$

The increase in the concentration of τ_s via the increase in the exciton $\langle V_g \rangle$ may be offset by the increased detrapping rate K_{so} with temperature. By contrast, the deep-trap concentration is given by

$$[\tau_d] = \frac{PK^{\text{ISC}}[S_0]}{(K_{s1} + K^{\text{ISC}})(K_E)} \left(\frac{K_{di}}{K_d} \right), \quad (6.19b)$$

and its temperature dependence results only from the increase in the group velocity of the exciton states with temperature. Finally, the temperature dependence of the *ratio* of the trap populations is only functionally related to K_{so} . This can be seen by combining Eqs. (6.18a) and (6.18b) in one case and (6.19a) and (6.19b) in another. In both cases, the ratio is

$$\frac{[\tau_s]}{[\tau_d]} = \frac{N_s}{N_d} \left(\frac{K_d}{K_s + K_{so}} \right). \quad (6.20)$$

This is valid for both conditions, $K_E \ll K_{di} + K_{si}$ and $K_E \gg K_{di} + K_{si}$. The important point of the above equations is that *the steady-state concentration of the shallow and deep traps and thus the emission intensity depends implicitly upon both the group velocities in the band and the rate of detrapping of the shallow-trap K_{so}* . Both of these quantities are measurable and provide, in principle, detailed information on the dynamics of trap-exciton interactions.

Qualitatively, the above processes can be physically viewed as follows. At very low temperatures both K_{so} and K_{do} are zero, and the populations $[\tau_s]$ and $[\tau_d]$ (except for changes caused by variations in $\langle V_g \rangle$) remain constant with increasing temperature. Since the shallow trap is closer in energy to the band than the deep trap, as the temperature is increased K_{so} becomes nonzero before K_{do} , and some of the shallow trap's population is thermalized into the exciton band. This additional exciton population migrates in the band at an average group velocity determined by the temperature and band dispersion, and is retrapped in deep traps. Contrary to what would have been expected for a thermal equilibrium, the deep trap gains population and intensity at the expense of the shallow trap. The importance of the deep-trap concentration in relation to the magnitude of K_{so} cannot be underestimated if a phenomenological understanding of the complexities and variations of impurity effects in crystals are to be properly understood.

C. Other considerations

To this point, the effects of possible differences in exciton and trap radiative and radiationless lifetimes on the temperature dependence of trap emission in the equilibrium temperature region have

not been discussed. If N_{tot} is the total triplet excited-state population, then $I_{\tau} \propto N_{\text{tot}}/z(T)$, where N_{tot} is assumed to be temperature independent. If the total lifetime of the exciton and trap states are equal then the transfer of population between the band and trap does not alter the value of N_{tot} . However, if they are not equal, N_{tot} will be temperature dependent, and $I_{\tau} \propto N_{\text{tot}}(T)/z(T)$. Hence, both N_{tot} and z are functions of temperature.

$N_{\text{tot}}(T)$ can be determined from a system of differential equations assuming steady state. In terms of the parameters in Fig. 12, assuming the ground-state concentration $[S_0]$ remains constant,

$$\frac{d[S^1]}{dt} = P[S^0] - K_{s1}[S^1] - K^{\text{ISC}}[S^1] = 0, \quad (6.21)$$

$$\frac{dN_{\text{tot}}}{dt} = K^{\text{ISC}}[S^1] - K_{\tau}\chi N_{\text{tot}} - K_E(1-\chi)N_{\text{tot}} = 0. \quad (6.22)$$

χ is the percentage of population found in the trap. $\chi = 1/z(T)$, and $(1-\chi)$ is the percentage of population found in the band at a given temperature. At steady state $N_{\text{tot}}(T)$ is found to be

$$N_{\text{tot}}(T) = \frac{1}{[K_{\tau}\chi + K_E(1-\chi)]} \left(\frac{K^{\text{ISC}}P[S^0]}{K_{s1} + K^{\text{ISC}}} \right), \quad (6.23)$$

where the only temperature-dependent parameter on the right side of the equation is χ . The ratio of the values of $N_{\text{tot}}(T)$ at two temperatures is

$$\frac{N_{\text{tot}}(T_2)}{N_{\text{tot}}(T_1)} = \frac{\{K_{\tau}\chi(T_1) + K_E[1-\chi(T_1)]\}}{\{K_{\tau}\chi(T_2) + K_E[1-\chi(T_2)]\}}. \quad (6.24)$$

Equation (6.24) can be used to obtain $N_{\text{tot}}(T_2)$ relative to the value of $N_{\text{tot}}(T_1)$, which may be used to normalize the total population for all other temperatures. Thus, it is not necessary to know the actual value of $N_{\text{tot}}(T)$. A similar procedure can be used in the case of more than one trap or for corrections in N_{tot} owing to spin-lattice relaxation effects discussed above.

Another point which needs to be mentioned is that it has been tacitly assumed that intersystem crossing takes place from the singlet exciton band to the triplet exciton band and that exciton migration and trapping takes place from the triplet band. However, in some cases after exciting initially into the singlet exciton band, migration and trapping take place before intersystem crossing occurs, producing triplet traps. If the triplet traps are in equilibrium with the band, the trap intensity as a function of temperature will reflect the parameters of the triplet system. However, if the time for a trap to transfer its excitation to the band is long compared to its lifetime for decay to the ground state, the triplet trap's population will be determined by the singlet trap's population. In this case, the problem must be considered in terms of the bandwidth and trap depth of the singlet exciton

and trap system, giving careful consideration to the question of equilibrium. In studying triplet systems, if these complications arise, they can be eliminated to a large extent by suitably filtering the excitation light so that only the first triplet excited state is produced.

D. Qualitative features of TCB in the non-Boltzmann region

The intensity-vs-temperature data for the two traps in deuterated d_2 -TCB crystals in the temperature region before Boltzmann equilibration (I) are illustrated in Fig. 11(a). The predicted behavior for a system of this type is indeed observed. The shallow-trap intensity decreases and the deep-trap intensity increases as the temperature increases. The shallow-trap hd -TCB and the deep-trap h_2 -TCB are 12.8 and 23.5 cm^{-1} below the d_2 -TCB triplet band ($k=0$), respectively. Because the Boltzmann factor is small in the temperature region of interest, there is a significant difference in the detrapping rates K_{s0} and K_{d0} . Apart from the phenomenological observation that the temperature dependences of the two traps qualitatively behave in the proper fashion in region I, several independent experimental observations conclusively demonstrate that $K_{s0} \gg K_{d0}$ for this system. In Fig. 13 the zero-field optically detected magnetic-resonance (ODMR) spectra²⁶ for the two traps found in deuterated TCB are illustrated. These

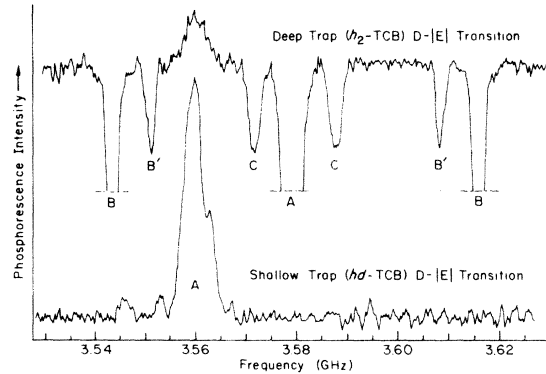


FIG. 13. Optically detected magnetic-resonance spectra for the deep trap (upper spectrum) and the shallow trap (lower spectrum) found in deuterated tetrachlorobenzene in the non-Boltzmann temperature region I. The A peaks are electron-spin-only transitions. The B and B' peaks are Cl^{35} and Cl^{37} electron-spin-plus-nuclear-quadrupole-spin transitions, respectively. The C peaks are electron-spin-plus- Cl^{35} - and Cl^{37} -double-nuclear-quadrupole-spin transitions. The large peaks in the deep-trap spectrum have been truncated to facilitate display. In the deep-trap spectrum between peaks B' and C on the low-frequency side is a peak going in the opposite direction from the rest of the deep-trap spectrum, and in the same direction and at the same frequency as the shallow-trap electron-spin-only transitions.

spectra are obtained by monitoring the optical emission to the electronic origin from the two traps separately as a microwave field is swept in frequency.²⁷ The upper spectrum is the optically detected electron zero-field $D-|E|$ transition of the deep trap, h_2 -TCB. The peak labeled *A* corresponds to electron-spin-only transitions while the peaks labeled *B* and *B'* are the simultaneous electron-spin-plus-³⁵Cl- and ³⁷Cl-nuclear-quadrupole transitions, respectively.^{28,29} The *B* and *B'* peaks are separated from the center line by the characteristic ³⁵Cl and ³⁷Cl excited-state nuclear quadrupole frequencies. The *C* peaks correspond to simultaneous electron-spin-plus-³⁵Cl- and ³⁷Cl-double-nuclear-quadrupole transitions.²⁹ These transitions are split from the electron-spin-only transition *A* peak by the difference in the ³⁵Cl and ³⁷Cl quadrupole frequencies. On the low-frequency side of the deep-trap spectrum between peaks *B'* and *C* is a peak going in the opposite direction from the rest of the spectrum at exactly the frequency associated with the shallow trap $D-|E|$ transition. This will be referred to as the *T* peak. The major peaks *A* and *B* of the deep-trap spectrum have been truncated to facilitate display. The lower spectrum in Fig. 13 is the $D-|E|$ transition of the shallow trap, hd -TCB. Only one peak is observed even at moderately high microwave powers at temperatures above 1.3 °K. This peak corresponds to the fully allowed electron-spin-only transition. The change in the light intensity in the shallow-trap spectrum is opposite the direction of the change in the light in the deep-trap spectrum except for the *T* peak. These results can be understood as follows.

The spin alignment of the shallow trap is changed by the application of the microwave field at the transition frequency, 3.5600 GHz. This change in spin alignment is at least partially carried into the exciton band by shallow-trap detrapping processes. The net result is that the exciton band acquires an altered spin alignment which is carried into the deep traps by the trapping process K_{dt} . This results in a change in the deep-trap light intensity in the same direction and at the same microwave frequency as the shallow-trap transition. This is the observed *T* peak in the deep-trap spectrum. Similar effects are observed in h_2 -TCB crystals when the exciton-band spin alignment is altered by a microwave field and the trap emission is monitored.³⁰ The significant point here is that there is no corresponding *T* peak in the shallow-trap spectrum even though the deep-trap transition is more than an order of magnitude stronger. This implies that the shallow-trap excitations are detrapping, migrating, and retrapping in deep-trap sites, but that deep-trap excitations are not transferring population to the shallow-trap sites to any

significant extent.

A second important observation can be made from the ODMR spectra. Because the electron-spin and the nuclear-quadrupole eigenstates are coupled by the electron-nuclear hyperfine interaction, only the pure electron transition will be observed in the *absence* of the hyperfine interaction. If the lifetime of a state is short compared to the inverse frequency associated with the hyperfine interaction, then the triplet state electrons will not be influenced by hyperfine interaction and the coupling of the electron eigenstates to the nuclear eigenstates will vanish, and the quadrupole peaks [$B(^{35}\text{Cl})$ and $B'(^{37}\text{Cl})$] will be absent from the ODMR. In TCB and similar compounds the hyperfine interaction is on the order of 1 MHz.^{29,30} The fact that quadrupole transitions are not observed in the shallow-trap ODMR spectrum sets an upper limit of less than 1 μsec for the time an excitation remains trapped in the shallow trap at 1.3 °K. On the other hand, the fact that strong quadrupole peaks are observed in the deep-trap ODMR spectrum implies that excitations remain in the deep traps for times much longer than 1 μsec . When the temperature is lowered to about 1.2 °K to decrease K_{so} , weak quadrupole satellites on the shallow-trap spectra appear at high microwave power, indicating that the detrapping rate constant K_{so} is in fact becoming smaller. Thus, the ODMR data, in addition to the temperature dependence of the trap emission data, establish that in the temperature region I immediately before Boltzmann equilibration occurs the shallow trap is detrapping rapidly while the deep trap is detrapping slowly relative to their lifetimes, i. e., $K_{so} \gg K_{do}$.

Finally, we would like to outline a method for measuring the absolute detrapping rate constants K_{so} and K_{do} by an optically detected magnetic-resonance experiment, in which the population entering the trap via K_{si} and K_{di} is completely removed from consideration. Specifically, it has been shown by Harris *et al.*³¹ that any state of the electron-spin coherence associated with the excited state and the full correlation function for dephasing of the electron-spin ensemble can be observed by the optical detection^{31,32} of electron-spin echoes³³ or spin locking.³⁴ By viewing the excited triplet state in an interaction representation which removes the electron-spin zero-field splitting it can be shown³⁵ that the population of one of the two spin sublevels being coupled by the time-dependent microwave field can be represented as a pseudomagnetization along the positive z axis of the interaction representation. Population in the other spin sublevel in the laboratory frame is related to a pseudomagnetization along the negative z axis of the interaction representation. When the time-dependent density matrix describing the dynamics

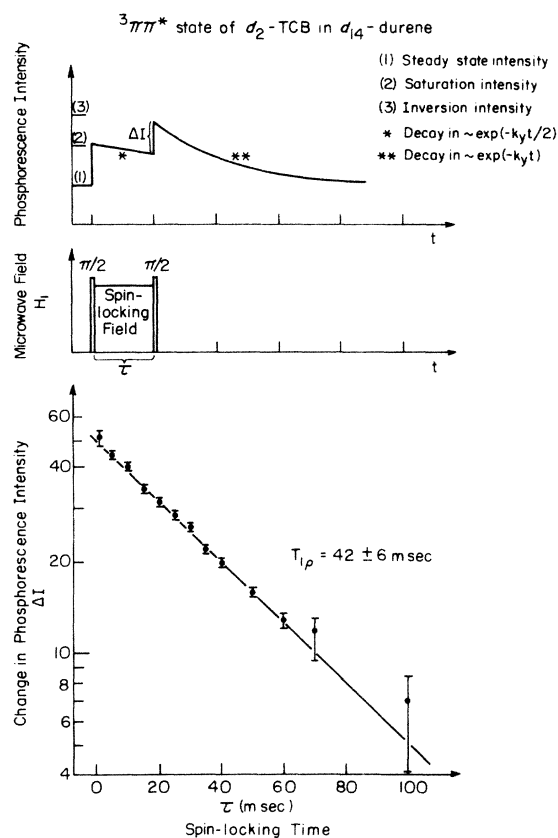


FIG. 14. (a) Relationship of the phosphorescence intensity to the pulse sequence used to spin lock. K_y refers to the total decay rate of the triplet-spin sublevel responsible for phosphorescence. (b) Microwave pulse sequence for spin locking. (c) Relaxation in the rotating frame, $T_{1\rho}$, for the $^3\pi\pi^*$ state of d_2 -TCB in d_{14} -durene at 2.0°K.

of the electron-spin ensemble is displayed through the electric dipole transition moment responsible for phosphorescence intensity, usually only z components of the interaction representation are observable³⁵ in the emission. In the present problem, the electron-spin coherence can be used to measure kinetic phenomena, such as the detrapping process, in a unique way. By applying a $\pi/2$ microwave pulse to one of the three zero-field transitions of a particular trap state, say the deep trap, the spin-sublevel populations become saturated in the laboratory frame but are still coherently coupled. The corresponding pseudomagnetization in the interaction representation is simply tilted 90° . Spin locking³⁴ the population in the rotating frame by phase shifting the applied microwave field 90° immediately after the $\pi/2$ pulse prevents the spin coherence prepared by the initial $\pi/2$ pulse from being lost for a time corresponding to $T_{1\rho}$. $T_{1\rho}$ can be measured³¹ by restoring the pseudomagnetization back to the z axis by an addi-

tional $\pi/2$ pulse with the same phase as the initial $\pi/2$ pulse and measuring the resulting change in phosphorescence, ΔI (cf. Fig. 14), as a function of the spin-locked time τ . The uniqueness of spin locking to the measurement of kinetic phenomena is that once the electron spins have been locked in the rotating frame any population entering the trap at later times via K_{si} or K_{di} enters along the plus or minus z axis in the rotating frame. The electron-spin coherence of this additional population is, however, lost very rapidly via rotary precession³⁶ in the plane perpendicular to the applied field in a time corresponding to the inhomogeneous relaxation time T_2^* . In short, in the rotating frame, this additional population never gets spin locked. The net effect in the laboratory frame is that any population entering the trap state after the initial $\pi/2$ pulse gets incoherently and equally distributed into both spin sublevels; hence, when the final $\pi/2$ pulse is applied to restore the spin-lock population, there will be no change in phosphorescence ΔI (cf. Fig. 14) due to the incoherent non-spin-locked population. Thus, $T_{1\rho}$ is identically equal to K_{so}^{-1} or K_{do}^{-1} when other contributions to relaxation are small compared to detrapping.

The ability to measure the absolute value for the detrapping rate constant or just a lower limit depends upon the magnitude of these other contributions. It has been already demonstrated³¹ that dephasing of a spin-locked ensemble due to fluctuating local fields (principally fields due to the nuclear spins) can be eliminated by the application of a locking field $\gamma\mathcal{H}_1$ large enough to ensure that the resonance condition in the rotating frame, $\gamma\mathcal{H}_1$, is larger than nuclear-electron dipole or hyperfine coupling. In effect, a large $\gamma\mathcal{H}_1$ eliminates contributions to the electron $T_{1\rho}$ from nuclear-spin diffusion. The only other serious limitation on $T_{1\rho}$, apart from the trap lifetime, is electron-spin-lattice relaxation T_1 . In the non-Boltzmann temperature region in the TCB system this is not a limitation on K_{so} . T_1 is on the order of the lifetime of the triplet state, while detrapping rates are three to four orders of magnitude faster. For deep traps, however, K_{do}^{-1} can approach the radiative and radiationless lifetime. This is illustrated in Fig. 14 for d_2 -TCB doped in d_{14} -tetramethylbenzene ($\Delta \sim 1450$ cm⁻¹). A $T_{1\rho}$ of 43 msec³⁷ at 2.0°K was found, a value representative of the lifetime of the triplet state. In the Y trap ($\Delta = 53$ cm⁻¹) in h_2 -TCB, however, the value for the loss of electron-spin coherence of ~ 600 μ sec³⁸ was found by a technique similar to spin locking. The details of these experiments will be reported later. Even at this initial stage of development, it is clear that experiments based on the measurement of electron-spin coherence in the rotating frame offer another new and unique method for studying

the dynamics of energy migration and, in this case, the absolute detrapping rates.

VII. RADIATIONLESS RELAXATION IN TRAP-EXCITON DECAY: A MODEL FOR DETRAPPING TO BAND STATES

In view of the central role the detrapping rate plays in achieving Boltzmann equilibrium, a concrete model for the detrapping process whose details can be verified and tested experimentally is desirable. In this context we develop a model in this section that describes detrapping to band states in a general way but includes in a well-defined and specific manner important considerations such as the phonon dispersions and populations, the exciton dispersion, and phonon-trap interactions. We will only consider single-phonon-single-trap interactions where the decay of the trap into the band conserves the total momentum and energy of the over-all process. Further we shall assume that the initial interaction of a phonon and trap results in an intermediate state that is degenerate with some k state in the band. The decay of the intermediate localized state into the delocalized band states is taken to be a radiationless relaxation process³⁹ and is displayed in the form of a Golden-Rule rate.⁴⁰ The assumptions implicit in this model are that the creation of the intermediate state is a stochastic process⁴¹ and that the decay of the intermediate trap state into the band states is irreversible in the sense that recurrence⁴² is negligible because of the high density of exciton states in the band and the finite lifetime of k states in the band into which the intermediate has evolved. This is schematically illustrated in Fig. 15.

In this model the probability per unit time of a trap $\langle \tau |$ interacting with a phonon $P(\epsilon)$ of energy ϵ and detrapping into a specific band state $\langle k |$ having momentum $\hbar k$ via an intermediate state τ_i is given by

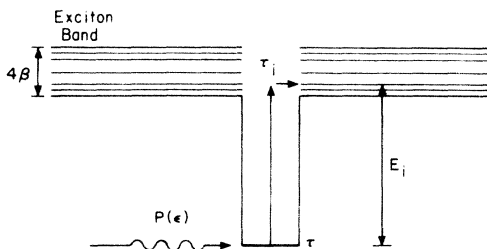


FIG. 15. Schematic representation of the detrapping process. $P(\epsilon)$ is a phonon of energy ϵ interacting with a trapped excitation τ to produce an excited trap state τ_i equienergetic with the i th exciton band state. The excitation then decays into the i th band state. E_i is the energy difference between the trap τ and the band state. The energy of the phonon $P(\epsilon)$ must obey $\epsilon \geq E_i$.

$$E_{ek} = (2\pi/\hbar) \langle n(\epsilon) \rangle_T |\langle \tau P(\epsilon) | \mathfrak{H}_{\text{TP}} | \tau_i P(\epsilon - E_i) \rangle|^2 \times |\langle \tau_i P(\epsilon - E_i) | \mathfrak{H}_{\text{TE}} | k P(\epsilon - E_i) \rangle|^2 \rho(E_i). \quad (7.1)$$

$\langle n(\epsilon) \rangle$ is the number of phonon states with energy ϵ ; $|\langle \tau P(\epsilon) | \mathfrak{H}_{\text{TP}} | \tau_i P(\epsilon - E_i) \rangle|^2$ is the probability of creating an intermediate τ_i which can be identified with $|\tau_i P(\epsilon - E_i)\rangle$. Both direct and Raman⁴³ trap-phonon interactions are included by $\epsilon = E_i$ and $\epsilon > E_i$, respectively. Obviously the initial phonons $P(\epsilon)$ must have energies greater than or equal to E_i unless multiphonon processes are included. The radiationless decay of the intermediate τ_i into the exciton manifold whose k states are at energies E_i above the trap is given by $|\langle \tau_i P(\epsilon - E_i) | \mathfrak{H}_{\text{TE}} | k P(\epsilon - E_i) \rangle|^2 \rho(E_i)$, where $\rho(E_i)$ is the exciton density-of-states function evaluated at E_i . We will assume that the final phonon $P(\epsilon - E_i)$ is not bound to or does not interact with the final exciton k state. With this assumption the intermediate trap-exciton coupling Hamiltonian \mathfrak{H}_{TE} does not depend upon coordinates of the phonon wave vectors, and hence only coordinates of the trap and band state need be considered. Although there are many mechanisms (i.e., many forms of \mathfrak{H}_{TE}) which could describe the coupling of the intermediate trap to the band, in the absence of experimental data it is not clear at this point what the most appropriate choice would be. The coupling matrix elements must certainly, however, reflect the exchange between the trap and band of both electronic energy and the local distortion that is adiabatically propagated with the excited state in the Frenkel limit.

The average number of phonons at energy ϵ at temperature T , $\langle n(\epsilon) \rangle_T$, is given by the Planck distribution function,⁴⁴

$$\langle n(\epsilon) \rangle_T = \frac{1}{e^{\epsilon/\hbar T} - 1}, \quad (7.2)$$

in which the phonon energies ϵ are given explicitly by the phonon dispersion of the crystal. The total detrapping probability per unit time, which is the detrapping rate constant K_{so} or K_{do} , is found by summing over all phonons of energy $\epsilon \geq E_i$ and then summing over all intermediate states τ_i which have energies E_i greater than or equal to the energy difference between the bottom of the band and the trap, i.e.,

$$K_{so} = \sum_k \sum_{\epsilon \geq E_i} E_{ek}. \quad (7.3)$$

When considering the temperature region in which K_{so} is just becoming nonzero, $E_i \gg kT$, the Planck distribution function can be approximated by

$$\frac{1}{e^{\epsilon/\hbar T} - 1} \approx e^{-\epsilon/\hbar T}. \quad (7.4)$$

Further, since the one-dimensional exciton den-

sity-of-states function $\rho(E_i)$ is sharply peaked at $k=0$ and $k=\pm\pi/a$, we anticipate that intermediate states τ_i with energies equal to the energies of the top and bottom of the band might be expected to play the dominant role in the transition probability. If detrapping occurs *selectively*¹⁴ to one k state, say $k=0$,⁴⁵ then the bandwidth-to-temperature ratio would be relatively unimportant. On the other hand, in the *absence*⁴⁶ of the k -dependent trap-exciton coupling, if the bandwidth is significant relative to kT , the populations of phonons with energies capable of producing intermediate states at the top of the band will be small compared to the number of phonons available to produce intermediate states at the bottom of the band. In this limit, the expression for K_{so} can be approximated by considering only one intermediate state at the bottom of the band (which will be $k=0$ or $k=\pm\pi/a$ depending upon the sign of β). In either of these limits, the expression for K_{so} becomes

$$K_{so} \propto C \sum_{\epsilon=E_i} \rho(\epsilon) e^{-\epsilon/kT} = C \rho(E_i) e^{-E_i/kT}, \quad (7.5)$$

where E_i is the energy of the intermediate state τ_i which coincides with the maximum density of states of the band in one case, or to the particular k state ($k=0$) in the band in the other. All the non-temperature-dependent terms except the density-of-states function have been collected into the constant C , with the assumption that the phonon-trap interaction is constant over a range of phonon energies ϵ close to E_i .

In either of the above two limits the temperature dependence of the detrapping rate would appear as an activated process with an Arrhenius-like activation energy E_i . In reality, however, there is no activation, and E_i simply reflects the phonon distribution. Moreover, when the densities of k states at the energy of the intermediate trap state differ, as would be the case in mixed crystals with exciton chains of varying lengths, the absolute value of the detrapping rate K_{so} or K_{do} would change via $\rho(E_i)$ [Eq. (7.5)]; however, the apparent activation energy E_i would stay constant except for small changes resulting from differences in the band dispersions for different finite chain lengths. An experimental investigation into the validity of this model is being pursued using some of the optically detected magnetic-resonance techniques described in Sec. VI.

VIII. EXPERIMENTAL

1, 2, 4, 5-tetrachlorobenzene (TCB) was purchased from Aldrich Chemical Co., recrystallized from ethanol and vacuum sublimed to remove residual solvent. The recrystallized TCB was vacuum sublimed into a zone-refining tube, repeatedly outgassed, and sealed under vacuum in a 10-mm-diam

tube. The sample was then zone refined for 600 passes at a rate of 1 cm/h. Only the center third of the zone-refined material was used.

Deuterated TCB was prepared as follows.⁴⁷ D_2O and SO_3 were reacted to form D_2SO_4 . D_2SO_4 and h_2 -TCB were then heated for 12 h in a sealed tube at 150 °C. The cold reaction mixture was poured onto cracked ice and the exchange product was filtered off, washed with water, and used as the starting material for the next exchange. Five successive exchanges were performed in this manner. The final product was washed thoroughly with water, recrystallized from ethanol, vacuum sublimed, and zone refined for 300 passes. Two separate batches were prepared in this manner.

The percentage of deuterium in each sample was determined in the following manner. An accurately weighed sample from each batch of the deuterated TCB was dissolved in a known amount of CS_2 . Known amounts of dioxane, $C_4H_8O_2$, were added until the concentration of protons from the two species in the CS_2 solution were approximately equal. Proton NMR spectra were then taken and integrated using a Varian model T60 NMR spectrometer. The spectra were also integrated mechanically by taking the area under the spectral peaks. Comparison of these areas allowed the computation of the percent of deuteration of the TCB. As a check on this procedure a second standard was used. A weighed sample of deuterated TCB was dissolved in a known volume of deuterated benzene 95.5% D. The deuterated benzene served as an internal standard in the analysis of the proton NMR spectra. Both of these procedures were repeated 6 times and gave the same result, although the standard deviation was smaller when using the dioxane standard. The deuterated TCB samples contained $97.5 \pm 0.1\%$ deuterium.

Since the deuteration procedure is limited by the percent deuteration of the D_2SO_4 , the deuterated TCB consisted of 3 species, h_2 -TCB, hd -TCB, and d_2 -TCB. Assuming that the substitution reaction proceeds with the same probability for exchange of either a hydrogen or deuterium atom with the ring, the percentage of the three species found in the sample can be determined by their statistical probabilities. A sample which contains 97.5% deuterium is composed of 95.06% d_2 -TCB, 4.88% hd -TCB, and 0.06% h_2 -TCB.

Quantities of both TCB and deuterated TCB were vacuum sublimed into individual crystal-growing tubes and outgassed. Single crystals were then grown using the Bridgman technique. The large single crystals were cleaved, and small transparent pieces were used as experimental samples. The samples were placed in a liquid-helium Dewar which was cooled slowly to 77 °K over a period of 30 min, after which liquid He was added. The tem-

perature was monitored by an NRC Equipment Corp. Alphatron vacuum gauge, type 530. The temperature can be read to 0.01 °K; however, a small systematic error in temperature measurement may occur if the crystal is not in complete thermal equilibrium with the liquid-helium bath. The temperature was varied between 4.2 and 1.35 °K by changing the rate of pumping on the liquid helium.

The samples were illuminated by a 100-W PEK high-pressure mercury arc lamp through a 2800-Å interference filter. Excitation takes place into the singlet manifold and after intersystem crossing the first excited triplet state is populated. Phosphorescent emission from the triplet state is detected at right angles to the exciting light using a $\frac{3}{4}$ -m Jarrell Ash Czerny-Turner scanning spectrometer with a cooled EMI 6256 photomultiplier tube. The spectrometer is also fitted with a camera which was used for absorption spectra to determine the exciton origin and trap depths. The phosphorescent emission spectrum of the h_2 -TCB samples consists of two electronic and vibronic origins, one from the exciton band, 3748.2 Å, and the other from a trap, 21.3 cm⁻¹ lower in energy. A detailed analysis of the phosphorescence spectrum has already been reported.^{11, 46} Although the exact nature of this trap is unknown, doping of impurities into TCB crystals does not enhance the intensity of this trap, but rather produces another trap of lower energy.⁹ The trap is thought to be associated with a crystal-lattice defect. At 4.2 °K, the d_2 -TCB spectrum consists of three phosphorescence origins, one from each of the three species found in the deuterated TCB crystal. The d_2 -TCB triplet-exciton-emission origin is at 3745 Å. The mono deuterated trap, hd -TCB, is 12.8 cm⁻¹ lower in energy, and the diproto trap, h_2 -TCB is 23.5 cm⁻¹ lower in energy than the exciton origin.

Optically detected magnetic resonance (ODMR) spectra of the trap in the TCB crystals and of the traps in the deuterated TCB crystals gave characteristic tetrachlorobenzene spectra. The details of the TCB trap's ODMR spectra and of the experimental setup are reported elsewhere.¹¹

The results of the trap-intensity-vs-temperature measurement are shown in Fig. 6 for the h_2 -TCB and in Fig. 11 for the d_2 -TCB traps. The figures are typical of several sets of data taken on separately prepared TCB single crystals and on single crystals prepared from each of the two batches of deuterated TCB.

Finally, all computer calculations illustrated in the figures and tables were performed on a CDC 7600.

IX. SUMMARY

(i) We have attempted to explain in a general way the mechanism by which thermal equilibrium be-

tween localized trap states and delocalized band states in solids is achieved. The essential feature of the statistical model which satisfactorily accounts for many experimental observations is that at low temperatures, exciton migration must propagate coherently as a wave packet rather than by a random-walk process in order to thermally equilibrate the exciton and trap states within the lifetime of the excited electronic state. A proper description of the process or processes related to the equilibrium populations of trap and band states must include the density of k states, the number of k states comprising the band relative to the number of localized trap states, the detrapping rates which are dependent upon phonon dispersions, the trap depth, the sign and magnitude of the intermolecular interaction which gives rise to the band dispersion, and phonon-exciton scattering.

(ii) The application of this model to crystals representative of one-dimensional bands allows one to extract from the temperature-dependent trap emission the magnitude of the band dispersion, the sign of the intermolecular interaction matrix element, and an estimate of the coherence length and average group velocity of the exciton wave packets.

(iii) In a crystal characterized by two or more trap states at different energies, below a certain temperature, a "bottleneck" in the Boltzmann distributions between band and trap states results because of the inability of the phonons to detrapp the deeper traps at a sufficient rate relative to the radiative and radiationless lifetimes of the state. We have solved the coupled differential equations and interpreted the various rate processes in terms of the coherent model.

(iv) We have derived a general theory for detrapping which treats the detrapping rate constant as a stochastic radiationless relaxation process in which the trap state once thermally activated decays irreversibly into the density of exciton states.

(v) Finally, we have presented a series of experiments on one-dimensional molecular crystals designed to test the model. Specifically, we have shown how electron-spin coherence and optically detected magnetic resonance in localized states can be used to obtain specific information regarding the dynamics of detrapping and the relationship of detrapping to Boltzmann equilibration between trap and band states.

ACKNOWLEDGMENTS

This work was supported in part by a grant from the National Science Foundation and in part by the Inorganic Materials Research Division of the Lawrence Berkeley Laboratory under the auspices of the U. S. Atomic Energy Commission.

*Alfred P. Sloan Fellow.

- ¹J. Frenkel, Phys. Rev. **37**, 17 (1931); Phys. Rev. **37**, 1276 (1931).
- ²A. Sommerfeld and L. Waldmann, *Hand- und Jahrbuch der Chemischen Physik—Die Boltzmannsche Statistik und Ihre Modifikation Durch die Quantentheorie* (Akademische Verlagsgesellschaft, Leipzig, 1939); R. C. Tolman, *The Principles of Statistical Mechanics* (Oxford U. P., Oxford, England, 1967).
- ³A. S. Davydov, *Theory of Molecular Excitons* (McGraw-Hill, New York, 1962).
- ⁴The singularities in the density-of-states function at $k = 0$ and $\pm \pi/a$ for infinite one-dimensional bands is not a problem when the number of exciton k states is limited by a finite number of molecules in the chain.
- ⁵R. S. Knox and A. Gold, *Symmetry in the Solid State* (Benjamin, New York, 1964).
- ⁶L. Pauling and E. B. Wilson, *Introduction to Quantum Mechanics* (McGraw-Hill, New York, 1935).
- ⁷L. van Hove, Phys. Rev. **89**, 1189 (1953).
- ⁸A. H. Francis and C. B. Harris, Chem. Phys. Lett. **9**, 181 (1971).
- ⁹A. H. Francis and C. B. Harris, Chem. Phys. Lett. **9**, 188 (1971).
- ¹⁰R. M. Hochstrasser and J. D. Whiteman, J. Chem. Phys. **56**, 5945 (1972).
- ¹¹A. H. Francis and C. B. Harris, J. Chem. Phys. **57**, 1050 (1972).
- ¹²(a) G. F. Koster and J. C. Slater, Phys. Rev. **95**, 1167 (1954); Phys. Rev. **96**, 1208 (1954); V. L. Broude and E. I. Rashba, Fiz. Tverd. Tela **3**, 1941 (1961) [Sov. Phys.-Solid State **3**, 1415 (1962)]; E. I. Rashba, Fiz. Tverd. Tela **5**, 1040 (1963) [Sov. Phys.-Solid State **5**, 757 (1963)]; V. L. Broude and S. M. Kochubei, Fiz. Tverd. Tela **6**, 354 (1964) [Sov. Phys.-Solid State **6**, 285 (1964)]. (b) J. Hoshen and J. Jortner, J. Chem. Phys. **56**, 933 (1972); J. Chem. Phys. **56**, 4138 (1972); J. Chem. Phys. **56**, 5550 (1972); P. Soven, Phys. Rev. **156**, 809 (1967); Phys. Rev. **178**, 1136 (1969); Phys. Rev. B **2**, 4715 (1970); H. K. Hong and G. W. Robinson, J. Chem. Phys. **52**, 825 (1970); J. Chem. Phys. **54**, 1369 (1970); H. K. Hong and R. Kopelman, J. Chem. Phys. **55**, 5380 (1971); D. P. Craig and M. R. Philpott, Proc. R. Soc. A **290**, 583 (1966); Proc. R. Soc. A **290**, 602 (1966); Proc. R. Soc. A **293**, 213 (1966).
- ¹³T. Holstein Ann. Phys. (N.Y.) **8**, 343 (1959); M. Grover and R. Silbey, J. Chem. Phys. **54**, 4843 (1971).
- ¹⁴R. W. Munn and W. Siebrand, J. Chem. Phys. **52**, 47 (1970). Applications (Wiley, New York, 1966), Vol. II.
- ¹⁵W. Feller, *An Introduction to Probability Theory and Its Applications* (Wiley, New York, 1966), Vol. II.
- ¹⁶C. B. Harris and M. D. Fayer (unpublished results).
- ¹⁷G. W. Robinson and R. P. Frosch, J. Chem. Phys. **37**, 1962 (1962).
- ¹⁸C. Dean, M. Pollak, B. M. Craven, and G. A. Jeffrey, Acta Crystallogr. **11**, 710 (1958).
- ¹⁹E. Kreyszig, *Advanced Engineering Mathematics* (Wiley, New York, 1967).
- ²⁰C. A. Hutchison, Jr. and B. W. Mangum, J. Chem. Phys. **34**, 908 (1961).
- ²¹A. C. Albrecht, J. Chem. Phys. **38**, 354 (1963).
- ²²D. S. McClure, J. Chem. Phys. **17**, 665 (1949).
- ²³A. A. Manenkov and R. Orbach, *Spin Lattice Relaxation in Ionic Solids* (Harper and Row, New York, 1966).
- ²⁴J. P. Wolfe, Chem. Phys. Lett. **10**, 212 (1971); U. Konzelman and M. Schwoerer, Chem. Phys. Lett. **18**, 143 (1973).
- ²⁵M. D. Fayer and C. B. Harris (unpublished results).
- ²⁶J. Schmidt and J. H. van der Waals, Chem. Phys. Lett. **2**, 640 (1968).
- ²⁷D. S. Tinti, M. A. El-Sayed, A. H. Maki, and C. B. Harris, Chem. Phys. Lett. **3**, 343 (1969).
- ²⁸M. J. Buckley and C. B. Harris, J. Chem. Phys. **56**, 137 (1972).
- ²⁹M. J. Buckley and C. B. Harris, Chem. Phys. Lett. **5**, 205 (1970).
- ³⁰A. H. Francis and C. B. Harris, J. Chem. Phys. **55**, 3595 (1971).
- ³¹C. B. Harris, R. L. Schlupp, and H. Schuch, Phys. Rev. Lett. **30**, 1010 (1973).
- ³²W. G. Breiland, C. B. Harris, and A. Pines, Phys. Rev. Lett. **30**, 158 (1973).
- ³³E. L. Hahn, Phys. Rev. **80**, 580 (1950).
- ³⁴A. G. Redfield, Phys. Rev. **98**, 1787 (1955); I. Solomon, C.R. Acad. Sci. (Paris) **248**, 92 (1959).
- ³⁵C. B. Harris, J. Chem. Phys. **54**, 972 (1971).
- ³⁶I. Solomon, Phys. Rev. Lett. **2**, 301 (1959).
- ³⁷C. B. Harris and H. Schuch (unpublished results).
- ³⁸C. B. Harris and R. L. Schlupp (unpublished results).
- ³⁹R. Kubo, Phys. Rev. **86**, 929 (1952); S. H. Lin, J. Chem. Phys. **44**, 3759 (1966); M. Bixon and J. Jortner, J. Chem. Phys. **48**, 715 (1968); J. Chem. Phys. **50**, 4061 (1969); D. M. Burland and G. W. Robinson, Proc. Natl. Acad. Sci. USA **66**, 257 (1970).
- ⁴⁰M. L. Goldberger and K. M. Watson, *Collision Theory* (Wiley, New York, 1964), Chap. 8.
- ⁴¹W. Feller, *An Introduction to Probability Theory and Its Applications* (Wiley, New York, 1966), Vol. I.
- ⁴²H. Poincaré, Acta Math. **13**, 67 (1890); R. M. Mazo, *The International Encyclopedia of Physical Chemistry and Chemical Physics* (Pergamon, Oxford, England, 1967), Vol. I; W. Siebrand, Chem. Phys. Lett. **14**, 23 (1972).
- ⁴³R. de L. Krönig, Physica (Utr.) **6**, 33 (1939); J. H. Van Vleck, Phys. Rev. **57**, 426 (1940); Phys. Rev. **57**, 1052 (1940).
- ⁴⁴R. C. Tolman, *The Principles of Statistical Mechanics* (Oxford U. P., Oxford, England, 1967), p. 512.
- ⁴⁵A model for selective k -dependent detrapping can be developed using partially localized crystal eigenfunctions which are solutions to the perturbed periodic potential problem [cf. Ref. 12(a)].
- ⁴⁶In substitutionally disordered crystals where the k states are appreciably mixed, one might have decay of the localized trap state into many k states of the band. Because of the high density of exciton states at $k = 0$ and $k = \pm \pi/a$, the rate of decay of the trap into the band might still be preferential to these states.
- ⁴⁷R. N. Renaud, D. Kovachic, and L. C. Leitch, Can. J. Chem. **39**, 21 (1961).
- ⁴⁸G. A. George and G. C. Morris, Mol. Cryst. Liq. Cryst. **11**, 61 (1970).